

Subsurface microbial community structure shifts along the geological features of the Central American Volcanic Arc

Marco Basili^{1,2,3}, Timothy J. Rogers¹, Mayuko Nakagawa⁴, Mustafa Yücel⁵, J. Maarten de Moor^{6,7}, Peter H. Barry⁸, Matthew O. Schrenk⁹, Gerdhard L. Jessen^{10,11}, Sabin Zahirovic¹², David V. Bekaert^{8,13}, Carlos J. Ramirez¹⁴, Deborah Bastoni², Angelina Cordone², Karen G. Lloyd^{1,15*}, Donato Giovannelli^{2,3,4,8,16,*}

¹ Department of Microbiology, University of Tennessee Knoxville, TN, USA

² Department of Biology, University of Naples "Federico II", Naples, Italy

³ Institute for Marine Biological Resources and Biotechnologies, National Research Council (CNR-IRBIM), Ancona, Italy

⁴ Earth-Life Science Institute, Tokyo Institute of Technology, Tokyo, Japan

⁵ Middle East Technical University, Institute of Marine Sciences, Mersin, Turkey

⁶ OVSICORI, Universidad Nacional, Heredia, Costa Rica

⁷ Department of Earth and Planetary Sciences, University of New Mexico, Albuquerque, USA

⁸ Marine Chemistry & Geochemistry Department, Woods Hole Oceanographic Institution

⁹ Department of Earth and Environmental Sciences, Department of Microbiology and Molecular Genetics, Michigan State University, MI, USA

¹⁰ Instituto de Ciencias Marinas y Limnológicas, Universidad Austral de Chile, Chile

¹¹ Center for Oceanographic Research COPAS COASTAL, Universidad de Concepción, Concepción, Chile

¹² School of Geosciences, The University of Sydney, Australia

¹³ CRPG, France

¹⁴ Servicio Geológico Ambiental (SeGeoAm), Heredia, Costa Rica

¹⁵ Earth Science Department, University of Southern California, Los Angeles, CA, USA

¹⁶ Department of Marine and Coastal Science, Rutgers University, New Brunswick, NJ, USA

*Co-corresponding authors: donato.giovannelli@unina.it, lloyd@usc.edu

This paper is a non-peer reviewed preprint submitted to EarthArXiv. The preprint has not yet been submitted for consideration to a peer review journal. Subsequent versions of this manuscript may have slightly different content. IF accepted by a journal, the final version of this manuscript will be available through the 'Peer-reviewed Publication DOI' link. Please feel free to contact the corresponding author for questions or comments.

Subsurface microbial community structure shifts along the geological features of the Central American Volcanic Arc

Marco Basili^{1,2,3}, Timothy J. Rogers¹, Mayuko Nakagawa⁴, Mustafa Yücel⁵, J. Maarten de Moor^{6,7}, Peter H. Barry⁸, Matthew O. Schrenk⁹, Gerdhard L. Jessen^{10,11}, Sabin Zahirovic¹², David V. Bekaert^{8,13}, Carlos J. Ramirez¹⁴, Deborah Bastoni², Angelina Cordone², Karen G. Lloyd^{1,15*}, Donato Giovannelli^{2,3,4,8,16,*}

¹ Department of Microbiology, University of Tennessee Knoxville, TN, USA

² Department of Biology, University of Naples "Federico II", Naples, Italy

³ Institute for Marine Biological Resources and Biotechnologies, National Research Council (CNR-IRBIM), Ancona, Italy

⁴ Earth-Life Science Institute, Tokyo Institute of Technology, Tokyo, Japan

⁵ Middle East Technical University, Institute of Marine Sciences, Mersin, Turkey

⁶ OVSICORI, Universidad Nacional, Heredia, Costa Rica

⁷ Department of Earth and Planetary Sciences, University of New Mexico, Albuquerque, USA

⁸ Marine Chemistry & Geochemistry Department, Woods Hole Oceanographic Institution

⁹ Department of Earth and Environmental Sciences, Department of Microbiology and Molecular Genetics, Michigan State University, MI, USA

¹⁰ Instituto de Ciencias Marinas y Limnológicas, Universidad Austral de Chile, Chile

¹¹ Center for Oceanographic Research COPAS COASTAL, Universidad de Concepción, Concepción, Chile

¹² School of Geosciences, The University of Sydney, Australia

¹³ CRPG, France

¹⁴ Servicio Geológico Ambiental (SeGeoAm), Heredia, Costa Rica

¹⁵ Earth Science Department, University of Southern California, Los Angeles, CA, USA

¹⁶ Department of Marine and Coastal Science, Rutgers University, New Brunswick, NJ, USA

*Co-corresponding authors: donato.giovannelli@unina.it, lloyd@usc.edu

Keywords: Subduction zone, microbial diversity, subsurface ecosystem, geobiology, hydrothermal systems

Abstract

Subduction of the Cocos and Nazca oceanic plates beneath the Caribbean plate drives the upward movement of deep fluids enriched in carbon, nitrogen, sulfur, and iron along the Central American Volcanic Arc (CAVA). These compounds fuel diverse subsurface microbial communities that in turn alter the distribution, redox state, and isotopic composition of these compounds. Microbial community structure and functions vary according to deep fluid delivery across the arc, but less is known about how microbial communities differ along the axis of a convergent margin as geological features (*e.g.*, extent of volcanism and subduction geometry) shift. Here, we investigate changes in bacterial 16S rRNA gene amplicons and geochemical analysis of deeply-sourced seeps along the southern CAVA, where subduction of the Cocos Ridge alters the geological setting. We find shifts in community composition along the convergent margin, with communities in similar geological settings clustering together independently of the proximity of sample sites. Microbial community composition correlates with geological variables such as host rock type, maturity of

hydrothermal fluid and slab depth along different segments of the CAVA. This reveals tight coupling between deep Earth processes and subsurface microbial activity, controlling community distribution, structure and composition along a convergent margin.

Main Text

Introduction

Subduction zones are the primary tectonic settings that transfer volatiles between Earth's surface and subsurface^{1,2}. Many of these volatiles, such as inorganic carbon and redox-active elements, are biologically reactive and can be used for biomass synthesis and energy production. Earth's subsurface harbors a vast microbial community limited by the depth of the 122 °C isotherm^{3,4}. However, our understanding of how deep life interacts with the heterogeneous distribution of volatiles fluxing through subduction zones is limited. Recently, the subsurface microbial community of a ~400 km subduction segment traversing the Central American Volcanic Arc (CAVA) has been shown to shift composition and metabolic properties in response to across-arc variation in fluxes of slab- and mantle-derived volatiles^{5,6}. However, the geological setting can also vary *along* the axis of a convergent margin, because of changes in the nature of the downgoing slab vs. the overriding plate, or other secondary features such as ridges or seamounts. Currently, it is unknown whether such along-axis geological variation drives changes in the microbial community.

Previous across-arc work shows that subsurface biosphere communities comprise a gradient of different chemosynthesis-based ecosystems due to different combinations of fluid sources and upper plate processes (e.g.,^{6,7}). Similar ecosystems have been observed in underwater mud volcanoes, where the delivery of magmatic gasses supports well-developed ecosystems⁸. At serpentinizing ophiolite systems, the geological setting drives variation in the subsurface microbial community through differential volatile deliveries⁹. The conversion of carbon into biomass by these chemosynthetic communities may even be sufficient to impact the overall carbon budget of the subducting margin^{5,7}, with implications for our understanding of the global carbon cycle over Earth's history.

Unique subsurface microbial communities have also been identified in the backarc of the Izu-Bonin subduction zone¹⁰ and Taupō Volcanic Zone¹¹, as well as the forearc of the Mariana convergent margin¹², the Sunda subduction zone¹³ and the Peru convergent margin¹⁴. A large-scale backarc study¹¹ determined that microbial diversity is primarily influenced by pH at temperatures

< 70 °C, with the effect of temperature becoming more significant for temperatures > 70 °C. These authors found an increase in community dissimilarities with distance between sites, with niche selection driving assembly on a local scale. Previous studies found changes in microbial communities across partial along-arc sections convergent margins of Costa Rica and Peru^{5,6,14}.

Costa Rica and Panama have complex geological settings due to the intersection of several tectonic plates (Fig. 1a; Caribbean, Cocos, Nazca, and the Panama microplate) and the Cocos Ridge¹⁵. This complex tectonic setting creates regional-scale along-arc differences that affect volatile fluxes. The most prominent tectonic features in the area are: a) the Middle American Trench; b) the Cocos Ridge, a submarine volcanic range formed by the Galapagos hot spot track that is subducted in southern Costa Rica; and c) the Panama Fracture Zone, a transform fault zone that defines the triple junction between the Cocos, Nazca, and Caribbean plates off the coast of southern Costa Rica and northern Panama. Costa Rica is traversed by four mountain ranges, with most volcanoes located in the Guanacaste and Cordillera Talamanca volcanic ranges^{16,17}. Central-Northern Costa Rica is characterized by basaltic-andesitic volcanism with multiple volcanic features such as thermal waters, acidic rivers or streams rich in sulfur, iron, and silicates¹⁶. In contrast to Costa Rica, Panama is characterized by a major left-lateral transform fault, along which the Nazca Plate is moving eastwards and is subducting beneath Colombia. This results in a slab window, where a break in the subducting slab allows for a greater mantle influence in the area¹⁵. The occurrence of this slab window notably explains the absence of arc volcanism and the relatively low seismic activity in Western Panama^{15,18}.

Within the CAVA, only a handful of hot springs have been microbiologically characterized^{5,6,19-21}. We sampled deeply-sourced fluids from natural springs and wells to investigate whether their microbial compositions differ by regional tectonic province across the CAVA. In oceanic settings, warm fluids emanating from hydrothermal vents can be used as windows to peer into the rocky seafloor habitat and characterize its microbial community²². Similarly, sampling freshly expressed fluids before they pool at the surface in terrestrial hot springs provides access to subsurface microbial communities that are flushed out by the deeply-derived fluids^{5,6,14,23,24}. Previous work has shown that common soil microbes and laboratory contaminants comprise only minority populations in these samples and do not correlate with the tracers of deeply-derived geochemical variables^{5,6,23}. Furthermore, deep fluid communities, as shown by relatively high ³He/⁴He, suggesting significant contributions from mantle volatiles, and other geochemical indicators of active hydrothermal activity (e.g., hydrothermally derived anions and cations)^{7,23-25}, do not overlap with the microbial communities in the surrounding soils²⁴. Here, we compare changes in subsurface microbial communities along a ~700 km section of the

CAVA spanning Costa Rica and Panama. Our results show that microbial community composition shifts significantly according to geological changes along the CAVA, supporting the fundamental role that tectonic processes play in shaping subsurface microbial ecosystems which in turn affect the composition and quantity of volatiles recycled between Earth's interior and its surface.

Results

Geophysical parameters changing across the sampled section of the CAVA

Principal component analysis (PCA) of the geophysical parameters of 48 springs clusters them into several groups (Fig. 1B). First, the eight southern Panama sites clearly separate from the rest of the dataset along the first axis of PCA (44.8% of the variation in the total dataset; Fig. 1B, yellow markers). The Panama sites are distinguished from the rest of the sites by the presence of a significant slab window resulting in heavy input of volatiles from the mantle without volcanoes¹⁵ (Supplementary Fig. 1). The rest of the sites span different parts of the subduction province (outer forearc, arc and backarc), but their geophysical attributes are also distinguished along-arc.

We grouped the sites into five subgroups based on subduction province, geophysical characteristics (PCA, Fig. 1B), depth to slab (Fig. 1C), and south/north regional classification: Outer forearc (9 sites), Volcanic arc (17 sites), Backarc (5 sites), Cordillera Talamanca (9 sites), and Panama (8 sites). These delineate both across-arc progression from outer forearc, to arc, to backarc, as well as along-arc progression from these subduction zone provinces to Cordillera Talamanca and Panama. Samples from the active volcanic arc areas exhibit higher temperatures (56.7 ± 17.5 °C, with maximum of 88.9 °C) than average (43.8 ± 15.9 °C for all sites of the subduction zone), with lower values in the backarc (28.0 °C), outer forearc (33.3 ± 1.07 °C), and Panama (36.0 ± 1.0 °C). Conversely, pH values are the lowest in the active volcanic arc area (5.0 ± 1.9), with maximum values reported in the outer forearc of Costa Rica (9.0 ± 1.0) and in Panama (7.9 ± 1.2) (Supplementary Fig. 2).

Geochemical characteristics

The diversity of host igneous rocks was obtained by analyzing elemental concentrations using the total alkali-silica (TAS) graph (Fig. 2A). The sampled sites encompass a wide spectrum of volcanic host rock types, ranging from basalt to rhyolite. The variability in SiO₂ content among the sites classifies the majority of host rocks as basalts and andesites, with a smaller subset exhibiting a more dacitic and rhyolitic composition. The primary rock compositions do not exhibit a significant correlation with the subgroups identified above (Fig. 2A).

Fluids were classified by their major anions²⁶ into: (i) acidic (pH 0 to 3) chloride-sulfate waters with direct input of magmatic gases (Fig. 2C, red and burgundy dots), (ii) sulfate-poor, peripheral geothermal waters (orange dots), intermediate in composition between deeply-derived chloride-rich waters and soda springs (purple dots) characteristic of volcanic flanks volcanic and forearcs (Fig. 2C), and (iii) alkaline (pH 7 to 10) outer forearc sites poor in both sulfate and chloride (Fig. 2C, blue dots), with the exception of sites CI and CL (Fig. 2C, yellow dots) which contain high sulfate possibly from seawater influence. The majority of sites contain peripheral geothermal waters or alkaline springs, and only a few of them are deep chloride or acidic waters. Cation concentrations (Mg^{2+} , Ca^{2+} , and Na^+ plus K^+ ; organized according to Giggenbach²⁷) differentiate between acidic arc volcanic sites (yellow dots) relatively enriched in Ca^{2+} , calcite hosted springs, and peripheral partially equilibrated waters. Flank geothermal sites and forearc springs (purple dots) define a trend away from the Ca^{2+} apex, likely due to fluid neutralization accompanied by precipitation of calcite. Indeed, large travertine mounds were observed at many of these sites. The outer forearc as well as some forearc sites fall near the Na^+K^+ apex, suggesting that these were mature deep fluids partially equilibrated with alkali-feldspars and clays (Supplementary Fig. 3). All the other sites are mature deep sites (green dots). Many of the geological and geochemical variables show a strong degree of collinearity (Supplementary Fig. 4).

Prokaryotic diversity and community composition

A total of 7,339,931 bacterial 16S rRNA gene amplicon reads comprising 36,534 amplicon sequence variants (ASVs) were obtained. Across all bacterial communities, the most abundant phylum is Proteobacteria (38.3 ± 22.6 %), mainly including Gamma- (26.7 ± 22.1 %) and Alphaproteobacteria (6.0 ± 7.9 %) (Fig. 3). Other highly represented phyla include Bacteroidetes (11.8 ± 10.0 %) and Chloroflexi (7.2 ± 6.8 %). Aquificae has a high relative abundance only in a few sites from the active volcanic arc, with abundances up to 95 % in PL and TC sediment samples and with lower abundances (7 to 48 %) in 5 fluid samples of the volcanic arc with high temperatures. The Shannon richness index is significantly higher (ANOVA, $p < 0.001$) in sediments (4.6 ± 1.2) than in fluids (3.4 ± 1.2), and only 15.7 % of the ASVs are shared between fluid and sediment samples (with 26.7 % exclusive to fluids and 57.6% to sediments). Alpha diversity is not significantly different between regional groups for either sediments or fluids (Supplementary Fig. 5, ANOVA, $p = ns$) or between different hosting rock types as identified by TAS (ANOVA, $p = ns$). Bacterial community composition of sediment and fluid samples cluster into several groups across regions and sample types (Fig. 3). A well defined cluster of Firmicute-dominated fluid samples (with relative abundances ranging from 35 % to 93 %) are

from deep human-made wells spanning multiple geographical regions: Panama (i.e., CI, CZ, and CV), Cordillera Talamanca (i.e. BS, LP, and LH) and backarc (i.e. CW, PX, and XF). In the non-well natural spring fluids, communities belonging to both fluid and sediment cluster into geographical groups with similar environmental (i.e., temperature and pH) and $^3\text{He}/^4\text{He}$ (reported as Rc/Ra values) (Fig. 3 and Supplementary Fig. 2). Most of these sites from Panama (yellow sites) cluster together and have abundant Bacteroidetes, Deltaproteobacteria, and Alphaproteobacteria. The active volcanic arc cluster (dark blue) contains a higher percentage of Aquificae, unidentified Proteobacteria, Chloroflexi, and unclassified phyla. The majority of the Cordillera Talamanca sites cluster together, with a similar phyla distribution to the others, but with a greater contribution from Proteobacteria. Costa Rica outer forearc sites cluster together, containing more Deltaproteobacteria, Nitrospirae, Chloroflexi, and Actinobacteria compared to other sites. The bottom set of clusters include the non-well sites from the backarc, but also sites from other regions. These clusters do not have dominating phyla driving their clustering, except for the absence of uncharacterized phyla. These clusters contain sites from similar geological regimes (Fig. 3, colored dots on the left), but not similar temperatures, pH values, or $^3\text{He}/^4\text{He}$ ratios (Fig. 3, heatmap values on the right).

A non-metric MultiDimensional Scaling (nMDS) ordination based on Jensen-Shannon Divergence ($k=3$, stress = 0.176, best solution repeated 5 times) shows a significant separation between communities belonging to different along-arc geographical areas (Fig. 4, Supplementary Figs. 6-8). Here, we observe the same clusters that were observed in the hierarchical clustering from Panama, the volcanic arc and outer forearc regions (Fig. 3), with a clear separation between outer forearc and volcanic arc sites compared to the rest of the samples. Sites belonging to the backarc and Cordillera Talamanca are not as well-separated from the other regions, in contrast to the result from the hierarchical clustering approach. Overall, these statistical analyses show shifts in the bacterial community structure along the CAVA convergent margin, with individual communities in each region being more similar to each other than to sites of other regions (Fig. 4). The spatial autocorrelation analysis was not significant despite having a low p-value due to the large number of datapoints (Supplementary Fig. 9, Mantel test, $r = 0.14$, $p < 0.01$, $n=2071$), suggesting that dispersal and site proximity are not driving the regional similarity observed. Microbial diversity is explained instead by region (ANOSIM, $r = 0.38$, $p < 0.001$) (Fig. 4A-C) and fluid geochemistry (ANOSIM, $r = 0.38$, $p < 0.001$) (Fig. 4D and 4E).

Linear vector fitting against the nMDS ordination (on all 3 axis) reveals that temperature and pH do not explain bacterial diversity changes in our dataset when analyzing fluids and sediments together (envfit, $p = \text{ns}$, Supplementary Table 2 and Supplementary Fig. 10). Despite this,

temperature significantly correlates with nMDS axis 1 ($N = 63$, $r = 0.77$, $p < 0.001$) and with pH along nMDS axis 2 ($N = 60$, $r = -0.51$, $p < 0.001$). Linear vector fitting identifies $^3\text{He}/^4\text{He}$ as one of the key variables correlating with nMDS axis 3 (envfit, $p < 0.01$, Supplementary Table 2), together with a number of covariates including several geophysical (envfit, $p < 0.019$, Supplementary Table 2) and rock trace elements (Ni, Dy and Y, $p < 0.01$, Supplementary Table 2). Bacterial community structure variations along nMDS axis 3 significantly correlate with $^3\text{He}/^4\text{He}$ ($N = 56$, $r = -0.31$, $p < 0.01$, Fig. 4C).

Discussion

Our sites span diverse geophysical, geological and geochemical regimes that cohesively vary along the CAVA: i) dip slab angle and subduction geometry, with steeper subduction in the north of Costa Rica; ii) changes in host rock geochemical composition and origin of volatiles, and iii) changes in geochemical and physicochemical parameters (like temperature, pH and water type) that are controlled by deep fluids and proximity to volcanic complexes. Collectively, these parameters support clear along-arc regional geological trends (Fig. 1).

Our 16S rRNA gene amplicon-based bacterial community analyses from fluids and sediments of 48 hot springs over ~700 km of the CAVA show regional differentiation of bacterial diversity based on the geological features both across and along the arc (Fig. 4). Geochemical parameters such as pH and temperature exert a primary control on community composition, in agreement with previous studies^{11,21,28–30}. This reflects their direct effects on bacterial physiology, but also their indirect effects by determining rock weathering, element partitioning during water:rock interactions, redox state, and chemical speciation. However, temperature and pH alone do not describe the full variation we observe in the bacterial community composition of subsurface-derived fluids and the sediments they wash over. Most of the microbial groups do not vary systematically with temperature and pH (Fig. 3), suggesting that their distribution across the convergent margin is not a simple function of these two parameters^{5,14}. Bacterial community composition also shifts across-arc with distance from the trench, progressing from the outer forearc, to the forearc, to the arc, following increasing distance from the subducting trench (DSub, Fig. 3, Supplementary Table 2). This agrees with previous findings from a subset of 18 sites from CAVA showing that shifts in deep volatile delivery support changes in chemolithoautotrophic pathways and the redox reactions that power subsurface respiratory pathways^{5,6,31}.

In addition to this across-arc variation, the microbial diversity also shows clear shifts with major geological changes along the convergent margin. Microbial community structure from CAVA natural springs clearly differentiate by region (Fig. 3). This regional pattern is upheld when populations in fluids or sediments are considered separately or together, suggesting that the freshly expressed fluids influence the microbial communities that collect at the seep orifice, where sediments are being continuously washed by the seeping fluids^{23,24}. Separation is visible between microbial communities of the Costa Rica outer forearc, active volcanic arc, and Panama, whereas the Cordillera Talamanca and backarc sites show less strong regional clustering (Fig. 4A, Supplementary Fig. 6-8). Alpha diversity is not significantly different between these regions (Supplementary Fig. 5), suggesting that any regional differentiation between geological regimes is driven by the types of microbes present, rather than the total number of different microbes.

This regional differentiation of the microbial community is explained in our dataset using a combination of geochemical and geophysical information. The $^3\text{He}/^4\text{He}$ ratio can be used as a proxy to disentangle the origin of the volatiles since the two isotopes have distinct origins with ^3He being cosmogenic while ^4He is produced radiogenically in Earth's crust^{25,32}. Along the CAVA, the $^3\text{He}/^4\text{He}$ ratios show varying degrees of mantle influence on the volatile origin (Supplementary Fig. 1). Microbial diversity significantly correlates with $^3\text{He}/^4\text{He}$ values in our dataset (Fig. 4C and Supplementary Table 2), suggesting that the geological origin of the volatiles exerts a major control on community structure. This statement is further supported by the correlation of beta diversity with geophysical variables known to covary along the CAVA region (Supplementary Table 2). Accordingly, the fluid geochemical composition reflects a strong influence of deep volatiles and interactions with the overriding crust, rather than in-mixing of surface-derived fluids (Fig. 2). Together, the degree of hydrothermal maturation and crustal influence drive the differentiation of subsurface fluids into different geochemical compositions which influence the microbial communities at each site. The fluids cover the full range of variation in these properties, spanning calcite-rich waters, soda springs, acidic, deep chloride, and peripheral geothermal waters (Fig. 2).

The fluids and sediments of the volcanic arc region have a higher relative abundance of Aquificae-related ASVs. Cultured representatives of this group are hydrogenotrophic chemolithoautotrophs with optimum growth temperatures between 65 °C and 95 °C^{33,34}, consistent with the highest temperatures for the area (Fig. 3). The availability of hydrogen, together with the high temperatures, might favor the presence of these thermophilic hydrogen-oxidizing microorganisms.

The similarity between the Panama sites and the Costa Rica backarc sites cannot be explained by temperature and pH, alone but is instead best explained by similarities in aqueous geochemistry, which is ultimately controlled by the composition of the underlying bedrock, and the origin of volatiles. A recent study showed that the rock composition in Panama and in the backarc of Costa Rica is influenced by the Galapagos mantle plume¹⁵, suggesting a common source for volatiles and trace elements used by microorganisms as important cofactors in metabolism³⁵. An exception to these regional trends is a cluster of mostly fluid samples from wells, which have a high abundance of Firmicutes (in particular Clostridiales). Members of the Firmicutes have previously been found in some of the deepest and oldest aquifers on Earth and other subsurface environments^{36,37}.

Besides the association of Aquificae with arc sites and Firmicutes with well fluids, no other single bacterial phylum shows clear regional trends. The observed trends are driven by changes at lower taxonomic levels than phyla. These changes are ultimately controlled by geological and geophysical parameters, significantly differentiating the microbial diversity in these contrasting regions. Given the collinearity of several of these variables with variations in latitude along CAVA (Supplementary Fig. 4), we considered whether the observed regional similarities are due to biogeographic patterns controlled by dispersal rather than the underlying geological features. Although dispersal can be an important driver of microbial community composition in hot springs¹¹ our results suggest that dispersal did not contribute significantly to changes in the bacterial composition at the large spatial scales of our study (Supplementary Fig. S9, Mantel test, $r = 0.14$, $p < 0.01$, $N = 2071$). The correlation between the similarity matrix and the pairwise geographic distance between the sites is weak in spite of the low p-value which is affected by the large number of observations³⁸, and driven by a low number of sites located in close proximity from each other (Supplementary Fig. S9).

Changes in the subsurface microbial diversity sampled through deeply-sourced seeps²³ have previously been related to changes in underlying geological and geophysical characteristics over smaller areas, such as northern Costa Rica^{5,6}, Peru¹⁴ and Brothers volcano on the Kermadec arc⁸, and similar large-scale differences in microbial diversity have been previously observed within single geological regimes in karst aquifers in Slovenia³⁹ and in hot springs in New Zealand¹¹, Yellowstone National Park^{40,41} and South China⁴². Our study shows that subsurface microbial populations shift along large spatial scales (~700 Km) that encompass major shifts in the geology of the convergent margin. Even when sites from different geological regimes along the axis of the CAVA are physically close to each other, they have microbial communities clustering according to their geological characteristics, rather than proximity.

In conclusion, our study shows significant changes in the subsurface microbial community composition along the CAVA. The observed regional differentiation is not shaped by any single environmental variable or phylum. Instead, it appears to be driven by the complex interplay of conditions and microbial communities present in each geographical region. Even though each region has similar ranges of pH and temperature, we suggest that regionality in microbial community composition is affected by: (i) direct magmatic degassing and mature hydrothermal activity in the Costa Rican active volcanic zone, as shown by helium and carbon isotopes¹⁰, (ii) volatiles derived from the slab during subduction in the outer forearc, notably oxidized aqueous sulfur⁶, (iii) volatiles from flat slab subduction in the Cordillera Talamanca, where the slab remains shallow well into its interaction with the mantle⁴³, and (iv) the absence of a slab in Panama, where the only volatiles are directly derived from the mantle and crust¹⁵. These factors ultimately influence the ecological niches available in the subsurface, controlling the community structure, composition and functions of the subsurface biosphere. Our work demonstrates that coupling between deep Earth processes and surface manifestation of subsurface activities⁴⁴ helps shape the microbial communities of subsurface ecosystems. Since previous results suggest that these microbial communities play a significant role in mediating the volatile cycling between the Earth interior and its surface^{5-7,14,45}, we conclude that these biology-geology feedbacks extend to the large along-arc spatial scale spanning major changes in the geological setting.

Material and methods

Site description and sampling. During two sampling campaigns in 2017 and 2018, 48 deeply-sourced seeps were sampled across Costa Rica and Panama in the Central American Volcanic Arc (CAVA) (Fig. 1A, Supplementary Table 1) following a large-scale approach²³. Additional information regarding the geology of the CAVA are provided in the Supplementary Online Materials. From each site, 0.5 to 2 liters of hydrothermal fluids venting from the subsurface and ~ 15 grams of nearby sediments were collected. All samples were natural springs except for the following artificial wells (La Estrella LE, Casa Valmor CV, PraxAir Well PX, Cahuita Well CW, Coiba Island CI, Bajo Mendes Well BW, and Laurel Well LW). Fluids were immediately filtered through Sterivex 0.22 μm filter cartridges (MilliporeSigma) and quick-frozen onsite in liquid nitrogen, along with sediments. Fluid samples were collected for trace metals, major ions, cations and dissolved inorganic carbon (DIC), as described in Fullerton et al⁵. These were combined with samples for gas composition and noble gas analyses as reported previously^{5,7}.

Aqueous, sediment and rock geochemistry. Detailed methods and limits of detection were previously reported⁵. Briefly, concentrations of anions and cations were determined via ion chromatography (Dionex AS4A-SC column, sodium hydroxide eluent and ASRS-I suppressor for anions and Dionex CS12-SC column, with methane sulfonic acid eluent and CSRS-I suppressor for cations). Two factors were obtained based on the ternary plot classification of the aqueous geochemical composition (cations and anions²⁷) of the fluids at each site (Fig. 2). The bulk composition of hosting rocks was derived from EarthChem (<https://www.earthchem.org/>)⁴⁶ by querying the database with the coordinate of each site. The obtained whole rock compositions were checked against geological maps of the area to confirm the provenance from the same geologic unit and rock type hosting the samples seeps. Rock geochemistry data were used to investigate the correlation with host rock type.

Noble gas geochemistry. Noble gas analyses were conducted in various labs, as described in Barry et al⁷ and Bekaert et al¹⁵, where the data were originally published.

Geophysical data. We derived the following data from GPLates⁴⁷: crustal thickness (CT), distance from oceanic transformation (DOT), slab dip (S.Dip), distance from earthquakes (DEQ), distance from hotspot (DHS), slab depth (S.Depth), convergence rate (ConvR), Convergence Obliquity (ConvObl), convergence age (ConvAge), distance from mid oceanic ridge (DMOR), distance from nearest volcano (DV), distance from nearest fault identified by the U. S. Geological Survey (DMUSGS), distance from earthquakes (DEQ), and distance from the continental shelf (DCS).

Community DNA extractions. DNA was extracted from Sterivex® filters and sediments using a modified phenol-chloroform extraction optimized for low biomass samples, as previously published⁵. Extracted DNA was sequenced for analysis of bacterial diversity after amplifying the bacteria-specific V4-V5 region of the 16S rRNA gene using primers 518F (CCAGCAGCYGCGGTAAN) and 926R (CCGTCAATTCNTTTRAGT, CCGTCAATTTCTTTGAGT, CCGTCTATTCCTTTGANT) (<https://vampls.mbl.edu/resources/primers.php>). Sequencing was carried out as part of the Census of Deep Life initiative within the Deep Carbon Observatory at the Marine Biological Laboratory sequencing facility (<https://www.mbl.edu/>) on an Illumina MiSeq platform for amplicons.

Bioinformatic and statistical analysis. Paired-end reads were imported and analyzed in RStudio⁴⁸ version 3.6 using the DADA2 package⁴⁹. Quality check and trimming of the reads were performed (see deposited code for details on the parameter used). To optimize the merging of reads from the two separate libraries (the 2017 and 2018 datasets were sequenced in two different sequencing runs), we followed the DADA2 workflow for Big Data with little adaptation.

Amplicon sequence variant (ASV) inference was performed on the dereplicated sequences after pooling samples and merging paired-end reads. Chimeric sequences were removed and prokaryotic taxonomy was assigned using a native implementation of the naiveBayesian classifier method against the silva database (v132; <https://www.arb-silva.de/documentation/release-132/>). ASVs were defined as clusters sharing 100% sequence identity⁵⁰. All subsequent statistical analyses, data processing and plotting were carried out in the R statistical software version 3.6, using the phyloseq, vegan, ggtern and ggplot2 packages⁵¹⁻⁵⁴. We obtained high-quality bacterial 16S rRNA gene libraries from 39 sediments and 35 fluid samples across the 48 hot spring sites. The count table, taxonomy assignment and phylogenetic tree were combined together with the environmental variables into a phyloseq object. Low prevalence ASVs (less than 5 reads), mitochondria, chloroplast-related sequences, common contaminants⁵⁵ and human pathogens were removed from the dataset as described previously^{56,57}, removing 17.14 % of the total reads. The ASV table was normalized to a common scale by transforming it to relative abundance within a sample and then multiplying this proportion by the median library size across all samples⁵⁸. Statistical testing among variations in bacterial community composition was carried out using the permanova analysis for the centroid of the groups (ADONIS) based on a distance matrix calculated using the Jensen-Shannon Divergence distance. Differences between groups were evaluated by One-way Analysis of Variance (One-way ANOVA) followed by Tukey's post hoc test. Non-metric MultiDimensional Scaling (nMDS) ordinations were used to identify geographical clustering and environmental explanatory variables using linear correlations of environmental vectors with the envfit function in vegan. The roles of different sampling factors in influencing the observed community patterns were tested using a permutation distance-based approach using the ANOSIM function of the vegan package. All p values were adjusted using the Holm correction for multiple hypothesis testing which reduces the probability of false positives. In order to test for the contribution of dispersal, we performed a correlation analysis using the Mantel test (Vegan package) between the beta-diversity matrix of the microbial composition and the pairwise distance (in km) between the sites. The test was repeated for the fluids and sediment samples separated and together setting the same site distance to 0 km.

Data availability

All the sequences analyzed in this study are available through NCBI under project PRJNA797441 and ENA under project accession PRJEB63479. A complete R script containing all the steps to reproduce our analysis is available at https://github.com/giovannellilab/Basili_et_al_Central_America_Convergent_Margin with DOI

<https://zenodo.org/doi/10.5281/zenodo.10578391> together with all the environmental and geochemical data.

References

1. Kelemen, P. B. & Manning, C. E. Reevaluating carbon fluxes in subduction zones, what goes down, mostly comes up. *Proc. Natl. Acad. Sci. U.S.A.* **112**, E3997-4006 (2015).
2. Bekaert, D. V. *et al.* Subduction-Driven Volatile Recycling: A Global Mass Balance. *Annual Review of Earth and Planetary Sciences* **49**, null (2021).
3. Magnabosco, C. *et al.* The biomass and biodiversity of the continental subsurface. *Nature Geoscience* **1** (2018) doi:10.1038/s41561-018-0221-6.
4. Merino, N. *et al.* Living at the Extremes: Extremophiles and the Limits of Life in a Planetary Context. *Front. Microbiol.* **10**, (2019).
5. Fullerton, K. M. *et al.* Effect of tectonic processes on biosphere–geosphere feedbacks across a convergent margin. *Nature Geoscience* **14**, 301–306 (2021).
6. Rogers, T. J. *et al.* Chemolithoautotroph distributions across the subsurface of a convergent margin. *ISME J* **1–11** (2022) doi:10.1038/s41396-022-01331-7.
7. Barry, P. H. *et al.* Forearc carbon sink reduces long-term volatile recycling into the mantle. *Nature* **568**, 487 (2019).
8. Reysenbach, A.-L. *et al.* Complex subsurface hydrothermal fluid mixing at a submarine arc volcano supports distinct and highly diverse microbial communities. *Proc. Natl. Acad. Sci. U.S.A.* **117**, 32627–32638 (2020).
9. Rempfert, K. R. *et al.* Geological and Geochemical Controls on Subsurface Microbial Life in the Samail Ophiolite, Oman. *Front Microbiol* **8**, (2017).
10. Trembath-Reichert, E., Butterfield, D. A. & Huber, J. A. Active seafloor microbial communities from Mariana back-arc venting fluids share metabolic strategies across different thermal niches and taxa. *ISME J* **13**, 2264–2279 (2019).
11. Power, J. F. *et al.* Microbial biogeography of 925 geothermal springs in New Zealand. *Nature communications* **9**, 1–12 (2018).
12. Curtis, A. C., Wheat, C. G., Fryer, P. & Moyer, C. L. Mariana forearc serpentinite mud

- volcanoes harbor novel communities of extremophilic archaea. *Geomicrobiology Journal* **30**, 430–441 (2013).
13. Schippers, A., Köweker, G., Höft, C. & Teichert, B. M. Quantification of microbial communities in forearc sediment basins off Sumatra. *Geomicrobiology Journal* **27**, 170–182 (2010).
 14. Upin, H. E., Newell, D. L., Colman, D. R. & Boyd, E. S. Tectonic settings influence the geochemical and microbial diversity of Peru hot springs. *Commun Earth Environ* **4**, 1–8 (2023).
 15. Bekaert, D. V. *et al.* High $^3\text{He}/^4\text{He}$ in central Panama reveals a distal connection to the Galápagos plume. *PNAS* **118**, e2110997118 (2021).
 16. Castellón, E. *et al.* Scattering of light by colloidal aluminosilicate particles produces the unusual sky-blue color of Río Celeste (Tenorio Volcano Complex, Costa Rica). *Plos one* **8**, e75165 (2013).
 17. Induni, G. E. A. *Los Volcanes de Costa Rica: Geología, Historia, Riqueza Natural y Su Gente.* (EUNED, 2011).
 18. Dzierma, Y. *et al.* The steeply subducting edge of the Cocos Ridge: Evidence from receiver functions beneath the northern Talamanca Range, south-central Costa Rica. *Geochemistry, Geophysics, Geosystems* **12**, (2011).
 19. Arce-Rodríguez, A. *et al.* Thermoplasmatales and sulfur-oxidizing bacteria dominate the microbial community at the surface water of a CO₂-rich hydrothermal spring located in Tenorio Volcano National Park, Costa Rica. *Extremophiles* (2019) doi:10.1007/s00792-018-01072-6.
 20. Rodríguez, A. & van Bergen, M. J. Superficial alteration mineralogy in active volcanic systems: An example of Poás volcano, Costa Rica. *Journal of Volcanology and Geothermal Research* **346**, 54–80 (2017).
 21. Uribe-Lorío, L. *et al.* The influence of temperature and pH on bacterial community

- composition of microbial mats in hot springs from Costa Rica. *MicrobiologyOpen* **8**, e893 (2019).
22. Deming, J. W. & Baross, J. A. Deep-sea smokers: Windows to a subsurface biosphere? *Geochimica et Cosmochimica Acta* **57**, 3219–3230 (1993).
 23. Giovannelli, D. *et al.* Sampling across large-scale geological gradients to study geosphere–biosphere interactions. *Frontiers in Microbiology* **13**, (2022).
 24. Cascone, M. *et al.* Deeply-sourced springs of the Argentina backarc as windows into the subsurface. *Submitted* (2024).
 25. Barry, P. H. *et al.* The Helium and Carbon Isotope Characteristics of the Andean Convergent Margin. *Frontiers in Earth Science* **10**, (2022).
 26. Giggenbach, W. F. Isotopic shifts in waters from geothermal and volcanic systems along convergent plate boundaries and their origin. *Earth and Planetary Science Letters* **113**, 495–510 (1992).
 27. Giggenbach, W. F. Geothermal solute equilibria. Derivation of Na-K-Mg-Ca geothermometers. *Geochimica et Cosmochimica Acta* **52**, 2749–2765 (1988).
 28. Inskeep, W. P., Jay, Z. J., Tringe, S. G., Herrgard, M. & Rusch, D. B. The YNP metagenome project: environmental parameters responsible for microbial distribution in the Yellowstone geothermal ecosystem. *Front. Microbiol.* **4**, 67 (2013).
 29. Podar, P. T., Yang, Z., Björnsdóttir, S. H. & Podar, M. Comparative analysis of microbial diversity across temperature gradients in hot springs from Yellowstone and Iceland. *bioRxiv* 841700 (2019) doi:10.1101/841700.
 30. Sharp, C. E. *et al.* Distribution and diversity of Verrucomicrobia methanotrophs in geothermal and acidic environments. *Environmental microbiology* **16**, 1867–1878 (2014).
 31. Paul, R. *et al.* Complex organic matter degradation by secondary consumers in chemolithoautotrophy-based subsurface geothermal ecosystems. *PLOS ONE* **18**, e0281277 (2023).

32. Hilton, D. R., Fischer, T. P. & Marty, B. Noble Gases and Volatile Recycling at Subduction Zones. *Reviews in Mineralogy and Geochemistry* **47**, 319–370 (2002).
33. Giovannelli, D. *et al.* Insight into the evolution of microbial metabolism from the deep-branching bacterium, *Thermovibrio ammonificans*. *eLife* **6**, e18990 (2017).
34. Sievert, S. & Vetriani, C. Chemoautotrophy at Deep-Sea Vents: Past, Present, and Future. *Oceanography* **25**, 218–233 (2012).
35. Hay Mele, B. *et al.* Oxidoreductases and metal cofactors in the functioning of the earth. *Essays in Biochemistry* **67**, 1–18 (2023).
36. Chivian, D. *et al.* Environmental genomics reveals a single-species ecosystem deep within Earth. *Science* **322**, 275–278 (2008).
37. Becraft, E. D. *et al.* Evolutionary stasis of a deep subsurface microbial lineage. *The ISME Journal* **15**, 2830–2842 (2021).
38. Lin, M., Lucas, H. C. & Shmueli, G. Research Commentary—Too Big to Fail: Large Samples and the p-Value Problem. *Information Systems Research* **24**, 906–917 (2013).
39. Slabe, M. O. *et al.* Key drivers of microbial abundance, activity, and diversity in karst spring waters across an altitudinal gradient in Slovenia. *Aquatic Microbial Ecology* **86**, 99–114 (2021).
40. Colman, D. R., Lindsay, M. R. & Boyd, E. S. Mixing of meteoric and geothermal fluids supports hyperdiverse chemosynthetic hydrothermal communities. *Nature Communications* **10**, 681 (2019).
41. Shock, E. L., Holland, M., Amend, J. P., Osburn, G. R. & Fischer, T. P. Quantifying inorganic sources of geochemical energy in hydrothermal ecosystems, Yellowstone National Park, USA. *Geochimica et Cosmochimica Acta* **74**, 4005–4043 (2010).
42. Guo, L. *et al.* Temperature governs the distribution of hot spring microbial community in three hydrothermal fields, Eastern Tibetan Plateau Geothermal Belt, Western China. *Science of The Total Environment* **720**, 137574 (2020).

43. Gardner, T. W., Fisher, D. M., Morell, K. D. & Cupper, M. L. Upper-plate deformation in response to flat slab subduction inboard of the aseismic Cocos Ridge, Osa Peninsula, Costa Rica. *Lithosphere* **5**, 247–264 (2013).
44. Cloetingh, S. *et al.* Coupled surface to deep Earth processes: Perspectives from TOPO-EUROPE with an emphasis on climate- and energy-related societal challenges. *Global and Planetary Change* 104140 (2023) doi:10.1016/j.gloplacha.2023.104140.
45. Giovannelli, D. *et al.* Subsurface life can modify volatile cycling on a planetary scale. *Memorie della Societa Astronomica Italiana* **92**, 60 (2021).
46. Lehnert, K. A., Walker, D. & Sarbas, B. EarthChem: A geochemistry data network. *Geochimica et Cosmochimica Acta* **71**, A559 (2007).
47. Müller, R. D. *et al.* GPlates: Building a Virtual Earth Through Deep Time. *Geochemistry, Geophysics, Geosystems* **19**, 2243–2261 (2018).
48. Racine, J. S. *RStudio: A Platform-Independent IDE for R and Sweave.* (JSTOR, 2012).
49. Callahan, B. J. *et al.* DADA2: High-resolution sample inference from Illumina amplicon data. *Nature Methods* **13**, 581–583 (2016).
50. Callahan, B. J., McMurdie, P. J. & Holmes, S. P. Exact sequence variants should replace operational taxonomic units in marker-gene data analysis. *The ISME Journal* **11**, 2639–2643 (2017).
51. Oksanen, J. *et al.* vegan: Community Ecology Package. *R package version 2.0-7* (2012).
52. McMurdie, P. J. & Holmes, S. phyloseq: An R Package for Reproducible Interactive Analysis and Graphics of Microbiome Census Data. *PLOS ONE* **8**, e61217 (2013).
53. Hamilton, N. E. & Ferry, M. ggtern: Ternary Diagrams Using ggplot2. *Journal of Statistical Software* **87**, 1–17 (2018).
54. Wickham, H. *Ggplot2: Elegant Graphics for Data Analysis.* (Springer-Verlag, New York, 2009).
55. Sheik, C. S. *et al.* Identification and Removal of Contaminant Sequences From Ribosomal

- Gene Databases: Lessons From the Census of Deep Life. *Front. Microbiol.* **9**, (2018).
56. Cordone, A. *et al.* Bacterioplankton Diversity and Distribution in Relation to Phytoplankton Community Structure in the Ross Sea Surface Waters. *Front Microbiol* **13**, 722900 (2022).
57. Cordone, A. *et al.* Surface Bacterioplankton Community Structure Crossing the Antarctic Circumpolar Current Fronts. *Microorganisms* **11**, 702 (2023).
58. McMurdie, P. J. & Holmes, S. Waste Not, Want Not: Why Rarefying Microbiome Data Is Inadmissible. *PLOS Computational Biology* **10**, e1003531 (2014).

Acknowledgments

The authors acknowledge the Biology Meets Subduction Project, funded by the Alfred P. Sloan Foundation and the Deep Carbon Observatory (G-2016-7206) to P.H.B., J.M.d.M., D.G., and K.G.L., with DNA sequencing from the Census of Deep Life. Additional support came from NSF FRES (Award# 21211637) to P.H.B., J.M.d.M. and K.G.L. U. S. Department of Energy, Office of Science, Office of Biological and Environmental Research, Genomic Science Program (DE-SC0020369 to K.G.L.). FONDECYT Grant 11191138 and COPAS COASTAL ANID FB210021 (ANID Chile) to G.L.J. D.G. was partially supported by funding from the European Research Council (ERC) under the European Union's Horizon 2020 research and innovation program Grant Agreement No. 948972—COEVOLVE—ERC-2020-STG. M.B. was funded by the EU CampusWorld scholarship from UNIVPM to visit the laboratory of K.G.L. in the framework of a research collaboration between K.G.L. and D.G. S.Z. was supported by Australian Research Council grant DE210100084, and Alfred P Sloan grants G-2017-9997 and G-2018-11296. GPlates development is funded by the AuScope National Collaborative Research Infrastructure System (NCRIS) program.

Contributions

MB, KGL and DG wrote the original draft, MB performed initial data analyses. Conceptualization and funding acquisition were performed by PHB, JMdM, MOS, GJ, DG and KGL. Formal analysis and visualization were performed by MB, KGL and DG. Investigations and data acquisition were performed by MB, TJR, MN, MY, JMdM, PHB, SZ, DVB, MOS, GLJ, CJR, DB, AC, KGL and DG. Writing and editing of the final draft was performed by all authors.

Competing interests

The authors declare no competing interests.

Figures

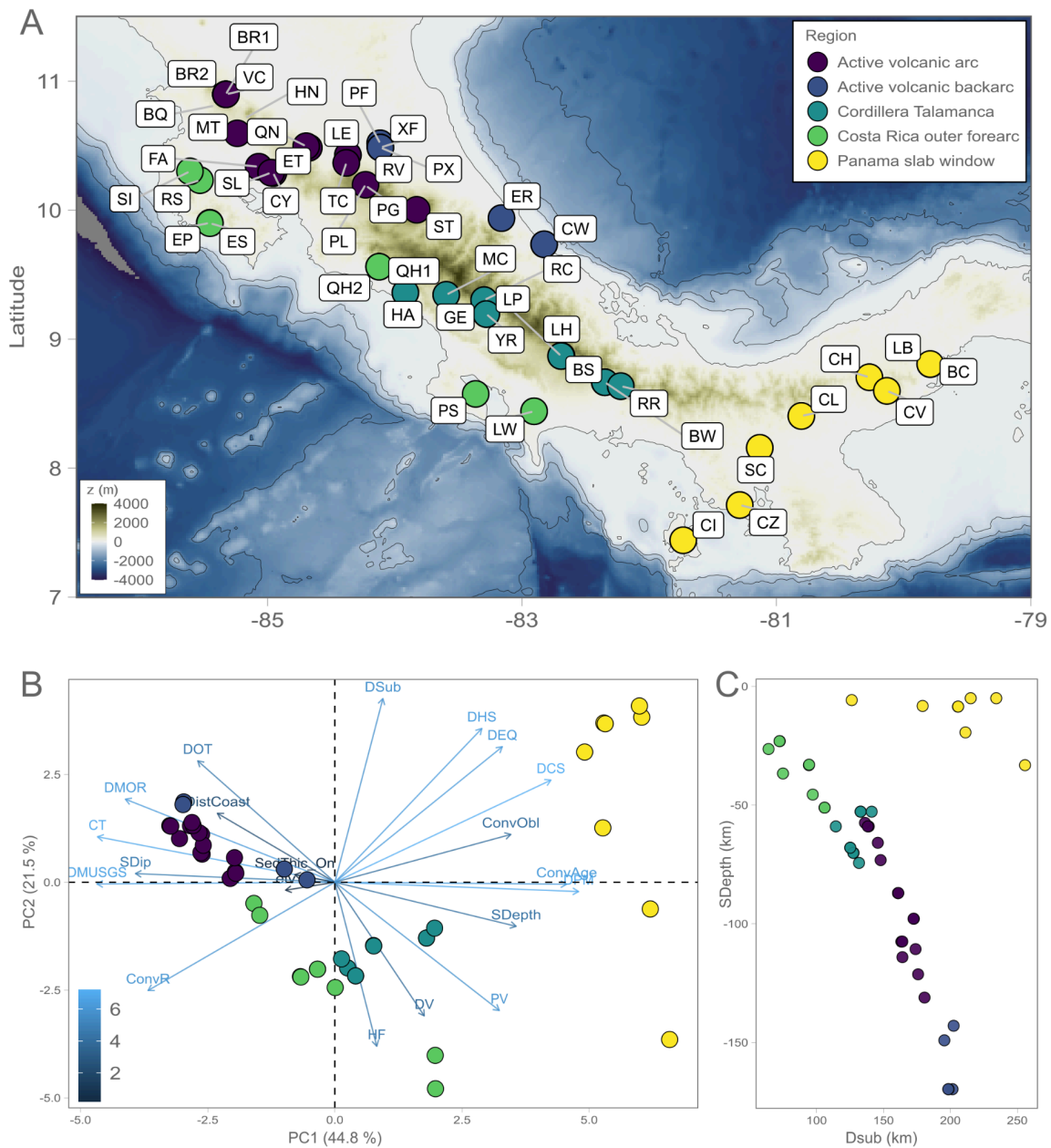


Fig. 1. Map and the sampled sites divided in regions and geophysical parameters defining each region. A Locations of the sampled seeps along the Central American convergent margin, from Costa Rica and Panama, depicting the bathymetry and the different plates that make up the region. Sites are colored by region. **B** Principal component analysis (PCA) showing the sites' clustering based on their geophysical characteristics. Vectors show the direction of change of the variable in the ordination space and the transparency of the vector is in accordance with the contribution to the corresponding orthogonal PCA axis. The percentage of variance explained is reported for each axis. DOT = Distance from oceanic transform, DistCoast = Distance from coastline, DMOR = Distance from Mid Ocean Ridge, CT = Crustal Thickness, SDip = Slab dip angle, DMUSGS = Distance from major faults, ConvR = Convergence rate, HF = heat flow, DV = Distance from volcanoes, PV = Plate velocities, SDepth = Slab depth, DPM = Distance from passive margin, ConvObl = Convergence obliquity, DCS = Continental shelf, DEQ = Distance from significant earthquake epicenter, DHS = Distance from hot spots, and Dsub = Distance from subduction trench. **C** Relationship between the slab depth (SDepth in km) and the distance from the trench (Dsub in km) for each of the sample sites showing the presence of a slab window under the Panama sites¹⁵.

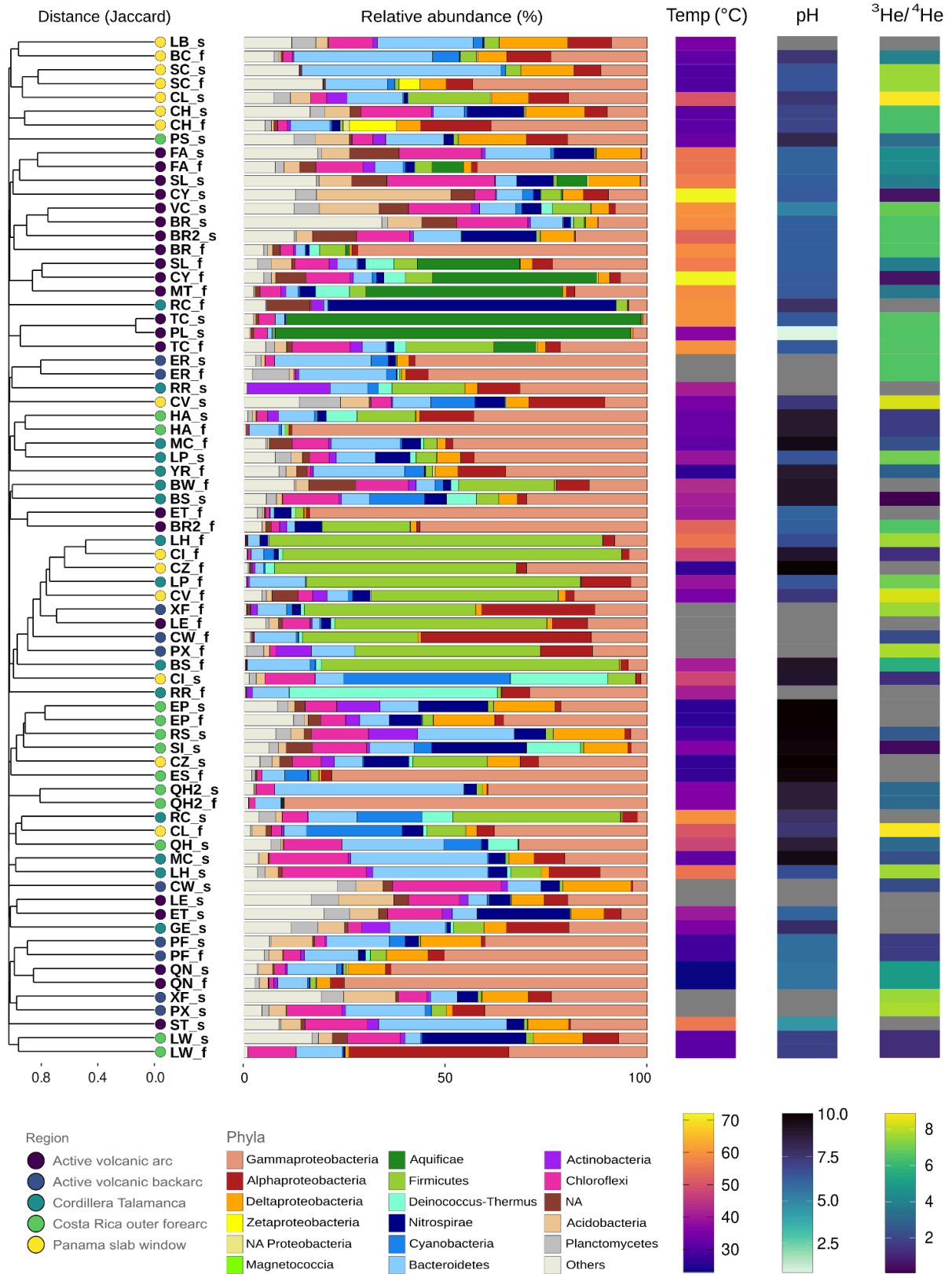


Fig. 3. Bacterial community composition, as shown by hierarchical clustering of Spearman Rank Coefficient based on 16S rRNA gene amplicon abundance. On the left, cluster analysis based on Jaccard similarities (method complete), with site codes colored by geographical area; on the center, a bar plot showing prokaryotic community composition at the Phylum level and Class level for Proteobacteria only. “Others” includes taxa aggregated with an average relative abundance <1 % across all samples, NA include the unidentified ASVs; on the right are environmental variables and geological settings: Temperature, pH, $^3\text{He}/^4\text{He}$; gray means no data.

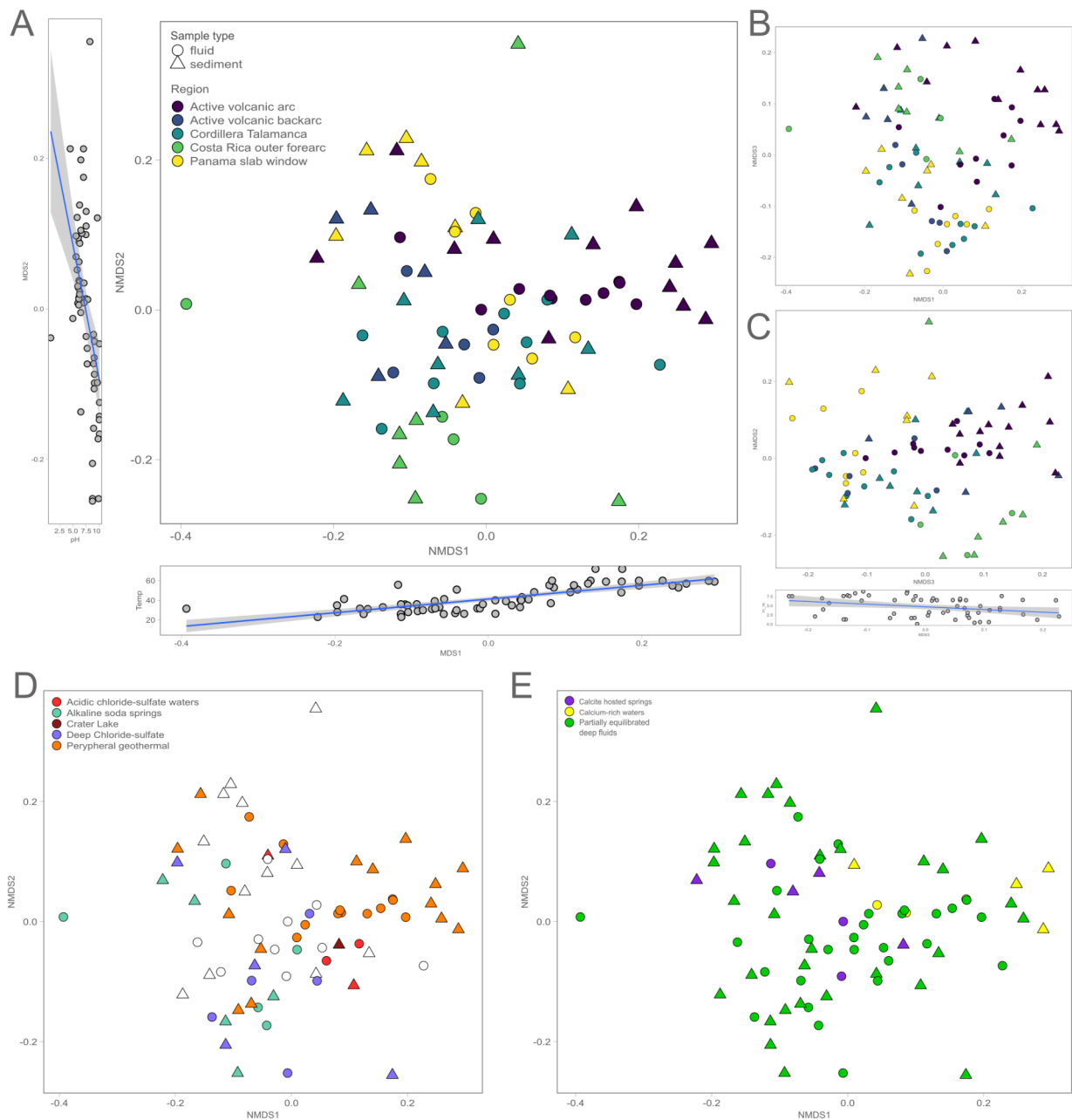


Fig. 4. Non-metric multidimensional scaling (nMDS) clustering of the sites based on bacterial community diversity and geochemical parameters. A nMDS plot of the 16S rRNA gene amplicon bacterial diversity based on Jaccard dissimilarity measure in the fluids (circles) and sediments (triangles), coloured by geographical area. Flanking plots show the relationship between nMDS1 and temperature ($r^2 = 0.77$, $p < 0.0001$, $n = 63$) and nMDS2 and pH ($r^2 = -0.50$, $p < 0.001$, $n = 60$). B and C, the same nMDS plot showing nMDS1 and nMDS3 (B) and nMDS2 and nMDS3 (C) with the relationship between nMDS3 and $^3\text{He}/^4\text{He}$ ($r^2 = -0.31$, $p < 0.01$, $n = 56$). D and E, the same nMDS plot in A, but colored according to the geochemistry-based grouping from anions (D) and cations (E). Empty symbols in D and E represent samples for which one or more ions were missing, and therefore have no placement in the ternary plot.

Supplementary Information

Supplementary Material and Methods

Geological context. The Cocos oceanic plate subducts beneath the Caribbean plate at a rate of 8-9 cm/yr, the Nazca oceanic plate converges eastward at 6 cm/yr relative to Northwestern South America (NWSA), and the Caribbean plate moves at 1-2 cm/yr to the E-SE relative to NWSA¹. The Panama block moves independently from both the Nazca and Caribbean Plates and is bounded to the north by subduction of the Caribbean Plate along a series of fold and- thrust belts called the Northern Panama Thrust Belt². Recent studies performed in southern Costa Rica and Panama suggest that the slab in the northwestern flanks of the Cocos Ridge dip gently (~20°) for approximately 100 km from the trench and abruptly steepen (up to 80°) farther downdip¹. There is (i) a significant difference in obliquity of the convergent margin between Costa Rica and Panama, (ii) a decreasing north/south gradient in thickness of the crust of the lower plate, and (iii) a potential increasing west/east gradient in slab dip and slab depth in accordance with distance from the subduction zone. All these changes contribute to variations in the volcanism along CAVA, with an interruption in active volcanism in Panama corresponding to a slab window^{1,2}.

Supplementary References

1. Bekaert, D. V. et al. High ³He/⁴He in central Panama reveals a distal connection to the Galápagos plume. PNAS 118, e2110997118 (2021).
2. Guillermo, A., Alvarado, & Cárdenes. Geology, Tectonics, and Geomorphology of Costa Rica: A Natural History Approach. in (2017).
3. Giggenbach, W. F. Geothermal solute equilibria. Derivation of Na-K-Mg-Ca geothermometers. Geochimica et Cosmochimica Acta 52, 2749–2765 (1988).

Supplementary Tables

Supplementary Table S1. Location and physico-chemical parameters of the sampled sites.

Code	Site name	Latitude	Longitude	Altitude	Region	Temperature	Salinity	pH	Dissolved Oxygen	³ He/ ⁴ He	Cl ⁻	SO ₄ ²⁻	DIC	Na ⁺	K ⁺	Mg ²⁺	Ca ²⁺	Rock type
		(°N)	(°E)	(m asl)		(°C)	(‰)		(%)	(Rc/Ra)	(ppm)	(ppm)	(ppm)	(ppm)	(ppm)	(ppm)	(ppm)	
BC	Los Bajos the Corera	8.806037	-79.790968	18	Panama slab window	31.8	23.87	7.5	51.0	4.0	165.54	0.42	56.85	56.46	1.52	2.09	0.27	Rhyolite
BQ	Borinquen	10.810883	-85.413707	535	Active volcanic arc	88.9	5.73	2.1	9.9	5.1	0.35	18.72	NA	0.73	0.19	2.23	3.92	Andesite
BR1	Blue River 2	10.898370	-85.328530	437	Active volcanic arc	59.0	3.25	6.2	7.0	6.5	29.03	4.23	9.56	9.28	3.03	11.56	5.85	Andesite
BR2	Blue River 1	10.898370	-85.328530	434	Active volcanic arc	53.0	3.25	6.2	41.0	6.5	16.75	3.72	9.31	5.52	1.75	6.75	5.45	Andesite
BS	Bajo Mendez Spring	8.666450	-82.349100	360	Cordillera Talamanca	40.9	3.10	9.1	20.0	5.7	NA	NA	NA	8.53	0.08	0.07	5.24	Andesite
BW	Bajo Mendez Well	8.665810	-82.348670	362	Cordillera Talamanca	43.2	3.13	9.1	3.0	NA	21.54	1.29	0.36	17.10	0.08	0.07	8.41	Andesite
CH	Chiguirí Abajo	8.705080	-80.269190	216	Panama slab window	31.1	15.30	7.0	41.0	6.4	74.96	16.87	37.97	72.42	1.60	1.64	2.05	Rhyolite
CI	Coiba Island	7.441040	-81.732770	50	Panama slab window	48.3	1.11	9.0	18.0	1.3	2.31	3.51	0.12	8.76	0.06	0.26	0.51	Basalt
CL	Calobre	8.404480	-80.803750	289	Panama slab window	50.9	3.26	7.5	29.0	8.9	6.93	9.98	0.74	19.36	0.15	0.38	3.99	Rhyolite
CV	Casa Valmor	8.599200	-80.131620	639	Panama slab window	34.9	3.75	7.5	14.0	8.4	21.93	0.19	0.89	15.05	0.17	2.43	0.58	Rhyolite
CW	Cahuita Well	9.735746	-82.825737	8	Active volcanic backarc	NA	NA	NA	NA	2.1	40.00	0.15	NA	45.21	0.19	0.60	0.74	Andesite
CY	Rio Cayuco	10.287497	-84.955524	184	Active volcanic arc	72.0	3.15	6.3	26.7	0.6	15.44	4.42	5.24	18.30	0.81	0.97	3.41	Basaltic Andesite
CZ	Salitral Carrizal	7.714070	-81.288320	60	Panama slab window	26.3	0.22	10.0	11.0	NA	0.03	0.09	0.86	3.36	0.06	0.27	0.78	Basalt
EP	Espabel	9.901885	-85.454327	126	Costa Rica outer forearc	26.0	0.10	10.0	4.0	NA	0.23	0.03	0.55	1.25	0.04	0.49	0.48	Basalt
ER	Rio Blanco Er Resbala	9.938223	-83.161331	89	Active volcanic backarc	NA	NA	NA	NA	6.5	12.52	0.43	NA	7.93	0.07	0.38	1.46	Picro Basalt
ES	Estrada	9.899005	-85.453514	122	Costa Rica outer forearc	27.0	0.11	9.8	48.3	NA	1.06	0.16	1.14	2.29	0.14	0.04	0.31	Basalt
ET	Eco Termales	10.484006	-84.675853	368	Active volcanic arc	40.0	0.97	6.0	13.4	NA	8.16	1.55	NA	4.29	0.65	3.64	1.75	Basaltic Andesite
FA	Finca Ande	10.336843	-85.069499	109	Active volcanic arc	55.0	2.97	5.9	10.3	4.4	20.37	6.19	14.22	25.04	1.67	1.67	2.66	Basaltic Andesite
GE	Gevi	9.194833	-83.280806	456	Cordillera Talamanca	35.8	0.45	7.8	85.0	NA	1.08	1.16	1.22	77.71	1.61	6.94	2.03	Basalt
HA	Hattillo	9.360220	-83.916640	118	Costa Rica outer forearc	33.0	4.97	8.9	26.0	1.7	27.38	9.88	0.12	20.43	0.24	1.34	7.12	Basalt
HN	Hornillas	10.712822	-85.177404	765	Active volcanic arc	87.9	7.09	1.8	57.0	6.7	0.24	12.00	1.12	0.53	0.17	0.58	1.32	Andesite
LB	Los Bajos	8.807360	-79.790610	26	Panama slab window	34.8	25.35	NA	70.0	NA	NA	NA	17.74	135.06	2.69	4.50	0.42	Rhyolite
LE	Las Estrella	10.427103	-84.368543	153	Active volcanic arc	NA	NA	NA	NA	NA	17.56	0.38	NA	11.37	0.62	2.40	14.06	Basalt
LH	Los Pozos Termales (hot)	8.870950	-82.689900	1676	Cordillera Talamanca	55.4	8.43	6.7	12.0	7.6	37.97	2.53	33.54	31.02	1.26	0.65	0.43	Andesite
LP	Los Pozos Termales (warm)	8.869660	-82.692820	1651	Cordillera Talamanca	39.1	5.88	6.5	32.0	7.0	30.45	1.74	31.33	30.18	1.49	0.94	1.36	Andesite
LW	Laurel	8.441190	-82.904870	32	Costa Rica outer forearc	31.5	0.55	7.1	3.5	1.2	0.15	0.01	7.11	1.97	0.26	0.76	0.48	Andesite
MC	Montecarlo - Bernardino	9.343910	-83.595650	812	Cordillera Talamanca	31.8	2.33	9.6	23.0	2.4	20.06	4.94	0.04	13.81	0.09	0.06	3.54	Basalt
MT	Mouse Trap	10.595774	-85.238451	166	Active volcanic arc	59.0	3.34	6.3	12.4	3.6	34.42	0.14	21.70	34.24	1.06	0.13	0.70	Rhyolite
PF	Pompilos finca	10.518466	-84.115180	53	Active volcanic backarc	28.0	1.96	5.8	4.3	1.7	17.50	0.18	23.72	12.38	1.10	6.31	0.81	Andesite
PG	Poas Volcano Laguna	10.188962	-84.227388	1632	Active volcanic arc	NA	NA	NA	NA	6.5	0.19	0.05	NA	0.11	0.03	0.16	0.20	Andesite
PL	Poas Volcano lake	10.196777	-84.229892	2334	Active volcanic arc	37.0	65.75	0.9	46.6	6.5	109.72	99.22	0.86	3.36	1.60	4.85	18.08	Andesite
PS	Playa Sandalo	8.575540	-83.364160	2	Costa Rica outer forearc	33.0	69.20	8.2	122.0	3.3	NA	NA	3.18	345.81	7.06	34.79	7.12	Andesite
PX	Praxair well 24	10.485523	-84.113229	68	Active volcanic backarc	NA	NA	NA	NA	7.8	16.78	0.57	NA	2.19	0.18	2.89	11.15	Basalt
QH1	Quepos Hot Springs 1	9.561710	-84.123251	298	Costa Rica outer forearc	48.0	1.39	8.7	47.3	3.1	25.21	2.06	0.10	17.02	0.23	0.02	4.86	Basalt
QH2	Quepos Hot Springs 2	9.561710	-84.123251	300	Costa Rica outer forearc	36.0	1.39	8.7	47.3	3.1	14.64	0.95	0.11	10.70	0.14	0.02	2.20	Basalt
QN	Quebrada naranja	10.495573	-84.696714	429	Active volcanic arc	23.0	0.10	5.6	84.0	4.9	0.31	0.03	2.81	0.46	0.12	0.29	0.73	Andesite
RC	Ujarasa	9.302830	-83.297820	943	Cordillera Talamanca	60.0	2.83	7.7	45.0	NA	NA	NA	1.07	15.90	0.20	0.21	1.81	Basalt
RR	Rockslide	8.635910	-82.223690	792	Cordillera Talamanca	41.3	2.51	NA	73.0	NA	NA	NA	0.32	8.96	0.11	0.09	5.84	Andesite
RS	Rancho el Salitral	10.232331	-85.531602	82	Costa Rica outer forearc	29.0	0.13	10.0	5.6	2.7	0.65	0.07	0.25	1.60	0.02	0.01	0.08	Rhyolite
RV	Recreo Verde	10.321576	-84.243686	557	Active volcanic arc	42.7	62.86	6.2	1.8	6.7	14.60	4.48	19.73	14.31	2.58	13.54	0.40	Basaltic Andesite
SC	El Salao Campollano	8.157550	-81.130970	136	Panama slab window	29.9	56.21	6.5	30.0	7.6	NA	NA	58.45	255.19	6.82	4.43	10.98	Basalt
SI	El Sitio	10.301239	-85.610549	36	Costa Rica outer forearc	36.0	1.82	9.8	36.2	0.4	0.64	0.03	2.24	1.11	0.03	0.02	0.15	Rhyolite
SL	Santa Lucia	10.290599	-84.972435	165	Active volcanic arc	57.0	1.46	6.1	22.0	3.8	3.52	5.02	5.69	11.83	0.54	1.07	2.74	Basaltic Andesite
ST	Santa Teresa	10.002942	-83.827507	2209	Active volcanic arc	55.8	2.98	4.5	4.7	NA	NA	NA	9.94	NA	NA	NA	NA	Andesite
TC	El Tucano bubbling site	10.366486	-84.381208	553	Active volcanic arc	60.0	1.84	6.3	18.7	6.6	18.53	0.06	13.57	12.96	1.31	2.29	1.06	Basaltic Andesite
VC	Blue River Volcancito	10.897847	-85.326461	436	Active volcanic arc	59.8	7.19	5.0	17.1	6.9	27.07	4.65	6.13	8.55	2.77	10.72	7.38	Andesite
XF	Praxair well 19	10.485523	-84.113229	74	Active volcanic backarc	NA	NA	NA	NA	7.6	NA	NA	NA	15.53	0.67	3.59	4.67	Basalt
YR	Yheri	9.194920	-83.280590	469	Cordillera Talamanca	26.0	4.59	8.9	10.0	2.9	NA	NA	0.06	28.90	0.28	0.28	7.51	Basalt

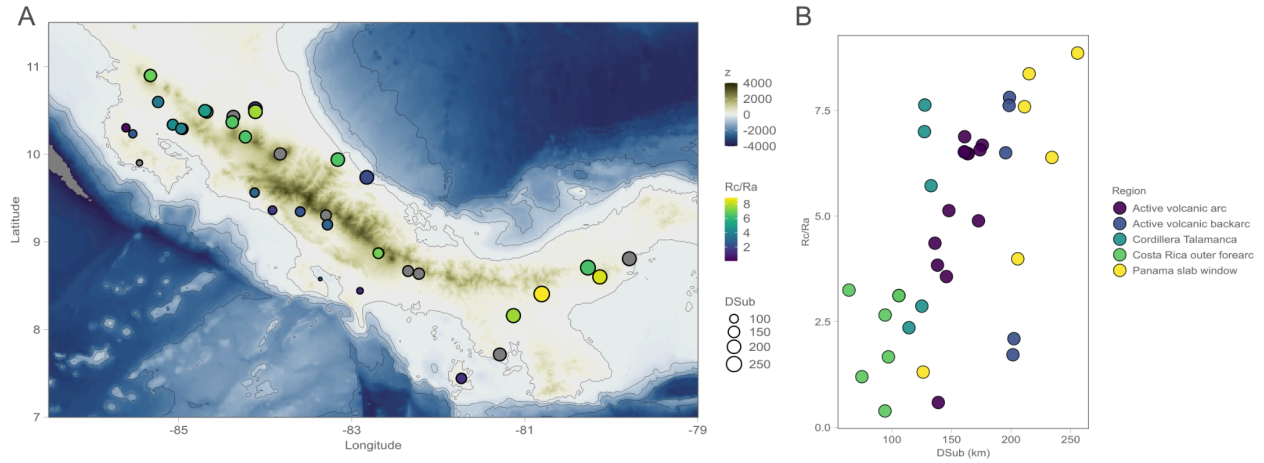
Supplementary Table S2. Envfit results against nMDS1, nMDS2 and nMDS3. Dsub = Distance from subduction, DOT = Distance from oceanic transform, DHS = Distance from hot spots, DV = Distance from volcanoes, DEQ = Distance from significant earthquakes, DCS = Continental shelf, SDepth = Slab depth, SDip = Slab dip angle, ConvR = Convergence rate and ConvObl = Convergence obliquity. One star (*); p-value less than 0.01, two stars (**) p-value is less than 0.001. Only variables with a p-value of less than 0.01 and a $r^2 > 0.32$ (for N=72) are marked in bold and considered statistically significant.

	Variable	NMDS1	NMDS2	r ²	Pr(>r)		NMDS1	NMDS3	r ²	Pr(>r)	
Location	latitude	0.2839	0.95885	0.1588	0.84167		0.06719	-0.99774	0.4172	0.591667	
	longitude	-0.32717	-0.94497	0.67	0.275		-0.95914	-0.28292	0.317	0.733333	
	Altitude	-0.35764	-0.93386	0.3141	0.76667		-0.25508	-0.96692	0.7729	0.233333	
	Variable	NMDS1	NMDS2	r ²	Pr(>r)		NMDS1	NMDS3	r ²	Pr(>r)	
Physico-Chemical	Temp	0.50604	-0.86251	0.913	0.18333		0.95382	0.30038	0.9012	0.1	
	Salinity	0.88148	0.47221	0.9712	0.09167		0.99138	0.13101	0.9671	0.1	
	pH	0.12583	-0.99205	0.9739	0.09167		0.9998	0.02003	0.8471	0.216667	
	DO	-0.23995	0.97079	0.9451	0.125		-0.72766	0.68594	0.9724	0.033333	
	TOC	-0.20459	-0.97885	0.6015	0.35833		-0.01544	-0.99988	0.4563	0.525	
	DIC	-0.11408	-0.99347	0.5904	0.43333		0.48306	-0.87559	0.3124	0.733333	
	CO2	0.23672	-0.97158	0.5994	0.38333		0.52539	0.85086	0.7969	0.191667	
	Rc/Ra	-0.29792	-0.95459	0.209	0.825		-0.15041	-0.98862	0.9999	0.008333	**
	Cl-	0.32508	-0.94569	0.716	0.31667		0.67862	-0.73449	0.7779	0.241667	
	SO42-	0.32475	0.9458	0.8157	0.23333		0.76162	0.64802	0.4133	0.45	
	Na+	0.07386	-0.99727	0.5132	0.50833		0.71114	0.70305	0.4898	0.516667	
	K+	0.70052	0.71363	0.4022	0.61667		0.28807	-0.95761	0.832	0.183333	
	Mg2+	0.35819	0.93365	0.255	0.675		0.17087	-0.98529	0.5739	0.45	
Ca2+	0.32844	0.94452	0.6632	0.38333		0.70802	-0.70619	0.3536	0.683333		
	Variable	NMDS1	NMDS2	r ²	Pr(>r)		NMDS1	NMDS3	r ²	Pr(>r)	
Geophysical	DPM	-0.92119	0.38912	0.0849	0.039		-0.38872	-0.92136	0.385	0.001	***
	CT	0.99362	0.11279	0.0563	0.121		0.35252	0.93581	0.3455	0.001	***
	SedThic On	-0.47271	-0.88122	0.002	0.914		-0.19124	-0.98154	0.0115	0.667	
	DistCoast	-0.58735	0.80933	0.0858	0.058		-0.96327	0.26853	0.0373	0.265	
	DSub	-0.0649	0.99789	0.201	0.001	***	-0.10618	-0.99435	0.0736	0.065	
	DMOR	0.97889	0.20436	0.0758	0.066		0.41753	0.90866	0.3297	0.001	***
	DOT	0.90511	0.42518	0.0956	0.029		0.52753	0.84954	0.2389	0.001	***
	DHS	-0.32829	0.94458	0.2397	0.001	***	-0.34206	-0.93968	0.2172	0.003	**
	DV	-0.32343	-0.94625	0.1671	0.006	**	-0.75568	-0.65494	0.0348	0.278	
	DMUSGS	0.87409	-0.48577	0.1024	0.017		0.39609	0.91821	0.4123	0.001	***
	DEQ	-0.4429	0.89657	0.1932	0.001	***	-0.41186	-0.91125	0.2176	0.002	**
	HF	-0.69084	-0.72301	0.0697	0.07		-0.78888	-0.61455	0.0552	0.123	
	PV	-0.64153	-0.7671	0.0857	0.039		-0.56331	-0.82624	0.1066	0.025	
	DCS	-0.3991	0.91691	0.1047	0.015		-0.24496	-0.96953	0.2637	0.001	***
	SDepth	0.2265	-0.97401	0.0042	0.871		0.06704	-0.99775	0.046	0.205	
	SDip	0.9033	0.42901	0.0123	0.657		0.30748	0.95156	0.0846	0.037	
	ConvR	0.26122	-0.96528	0.107	0.021		0.20437	0.97889	0.1696	0.001	***
	ConvObl	-0.50669	0.86213	0.0377	0.249		-0.24096	-0.97053	0.1533	0.003	**
	ConvAge	-0.89875	0.43847	0.0987	0.019		-0.41248	-0.91097	0.3849	0.001	***
	Variable	NMDS1	NMDS2	r ²	Pr(>r)		NMDS1	NMDS3	r ²	Pr(>r)	
Rock major	sio2 d	-0.12496	0.99216	0.0832	0.053		-0.28935	-0.95722	0.0056	0.826	
	tio2 d	-0.33172	-0.94338	0.103	0.033		-0.93815	-0.34623	0.0193	0.515	
	al2o3 d	0.27741	0.96075	0.0807	0.05		0.27437	0.96162	0.0807	0.057	
	FEOT d	0.39821	-0.91729	0.1165	0.016		0.86367	0.50405	0.0245	0.456	
	mno d	0.1395	-0.99022	0.0111	0.671		0.10269	0.99471	0.0052	0.859	
	mgo d	0.22973	-0.97325	0.1651	0.007	**	0.68906	0.7247	0.0138	0.63	
	cao d	0.33713	-0.94146	0.1552	0.004	**	0.60029	0.79978	0.0396	0.263	
	na2o d	-0.39293	0.91957	0.3285	0.001	***	-0.45298	-0.89152	0.1863	0.002	**
	k2o d	-0.7348	0.67829	0.0784	0.064		-0.72614	-0.68755	0.0746	0.084	
	p2o5 d	-0.99194	-0.1267	0.0547	0.146		-0.99925	-0.03871	0.0541	0.172	
	Variable	NMDS1	NMDS2	r ²	Pr(>r)		NMDS1	NMDS3	r ²	Pr(>r)	
Rock trace	Cu	0.70491	0.7093	0.0618	0.667		0.14998	-0.98869	0.2789	0.109	
	Co	0.78381	0.621	0.079	0.602		0.20264	-0.97925	0.3124	0.07	
	Mo	0.82472	0.56554	0.0867	0.57		0.22382	-0.97463	0.3282	0.064	
	Ni	-0.61896	0.78542	0.4453	0.029		-0.56689	0.82379	0.6356	0.002	**
	V	-0.94336	-0.33177	0.1208	0.44		-0.29391	0.95583	0.3869	0.044	
	Zn	-0.64882	-0.76094	0.0725	0.637		-0.16609	0.98611	0.2601	0.112	
	Ba	-0.90248	0.43073	0.1151	0.453		-0.32165	0.94686	0.3343	0.067	

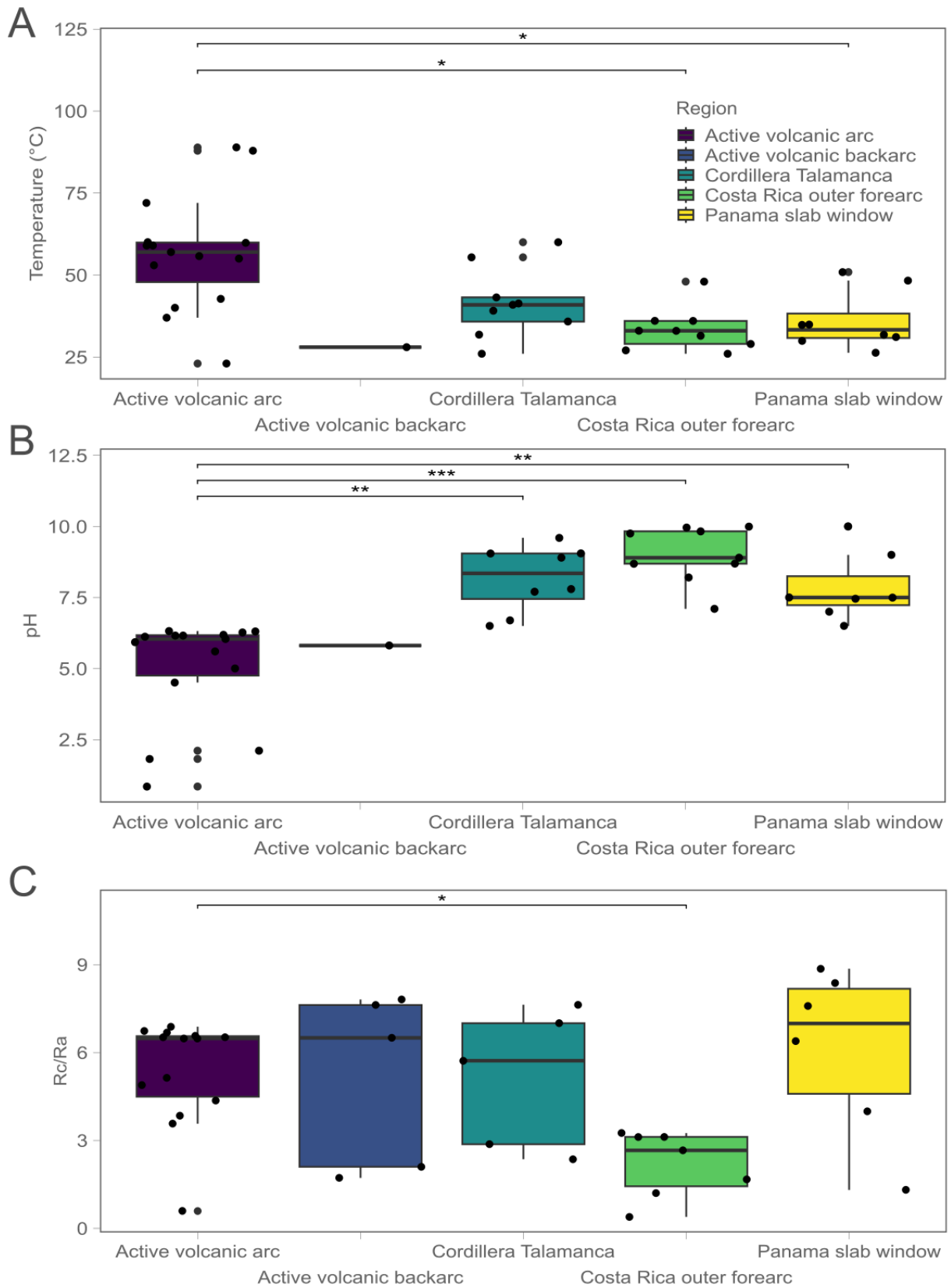
	Variable	NMDS1	NMDS2	r ²	Pr(>r)		NMDS1	NMDS3	r ²	Pr(>r)	
	Ce	-0.78144	0.62398	0.2354	0.18		-0.43221	0.90178	0.4799	0.011	.
	Cr	0.19926	-0.97995	0.0936	0.478		0.73015	0.68328	0.077	0.572	
	Dy	0.97266	-0.23224	0.2432	0.162		0.44295	-0.89655	0.5209	0.008	**
	Er	-0.35206	-0.93598	0.0612	0.698		0.05518	0.99848	0.1757	0.263	
	Eu	-0.87308	-0.48758	0.0804	0.593		-0.21787	0.97598	0.3288	0.071	
	Gd	-0.55118	-0.83439	0.0317	0.803		-0.03687	0.99932	0.1991	0.228	
	Ho	-0.18934	-0.98191	0.0908	0.563		0.24048	0.97065	0.1317	0.382	
	La	-0.48244	0.87593	0.3541	0.08		-0.57862	0.8156	0.4491	0.025	
	Lu	0.80468	0.5937	0.0828	0.584		0.21358	-0.97693	0.3204	0.067	
	Nb	-0.01062	0.99994	0.2385	0.186		-0.85877	-0.51235	0.0792	0.594	
	Nd	-0.93353	0.35851	0.1756	0.291		-0.3682	0.92975	0.4486	0.019	.
	Pb	0.80573	0.59229	0.0832	0.582		0.2144	-0.97675	0.3208	0.067	
	Pr	-0.00554	0.99998	0.2014	0.243		-0.92979	-0.36809	0.0585	0.68	
	Rb	-0.5489	0.83589	0.0984	0.485		-0.36735	0.93008	0.2083	0.212	
	Sm	-0.86978	0.49344	0.1235	0.419		-0.33551	0.94204	0.3391	0.066	
	Sr	0.03572	0.99936	0.1807	0.293		-0.55241	-0.83357	0.1079	0.468	
	Ta	0.76561	0.6433	0.0775	0.609		0.19672	-0.98046	0.3065	0.076	
	Tb	-0.14256	-0.98979	0.081	0.59		0.29141	0.9566	0.1238	0.405	
	Th	0.07484	0.9972	0.1176	0.469		-0.81833	-0.57475	0.0235	0.87	
	U	0.39879	0.91704	0.0684	0.688		0.03642	-0.99934	0.1209	0.415	
	Y	0.63262	-0.77446	0.5418	0.011		0.6158	-0.7879	0.7192	0.001	***
	Yb	0.93756	0.34783	0.1167	0.455		0.28633	-0.95813	0.3823	0.046	
	Zr	-0.25067	0.96807	0.1661	0.288		-0.60514	0.79612	0.1515	0.322	

Supplementary Figures

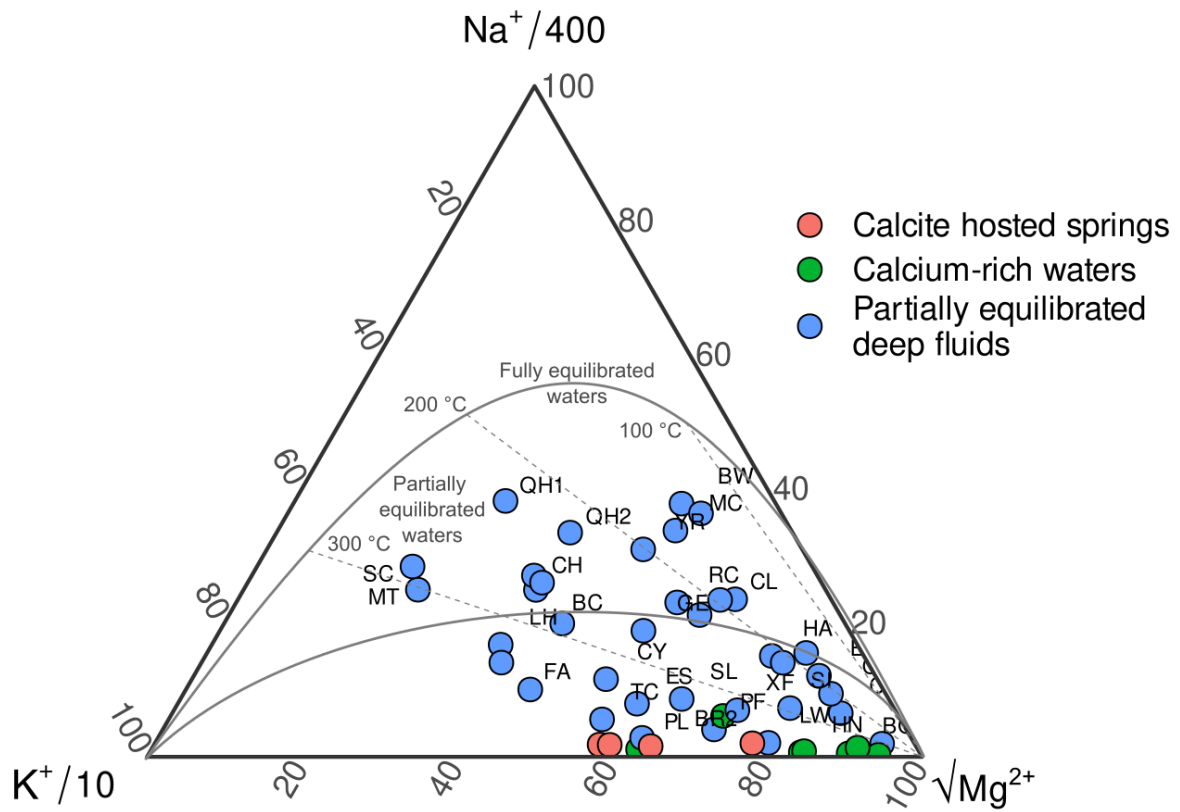
Supplementary Fig. S1. Changing in volatile sources in the sample dataset as shown by the $^3\text{He}/^4\text{He}$ ratio expressed as Rc/Ra . A $^3\text{He}/^4\text{He}$ and distance from subduction (in km) across the sampled area; B Regression analysis depicting positive relationship between distance from subduction and $^3\text{He}/^4\text{He}$ ratio (Rc/Ra) ($r = 0.59$, $p < 0.001$, $n = 34$).



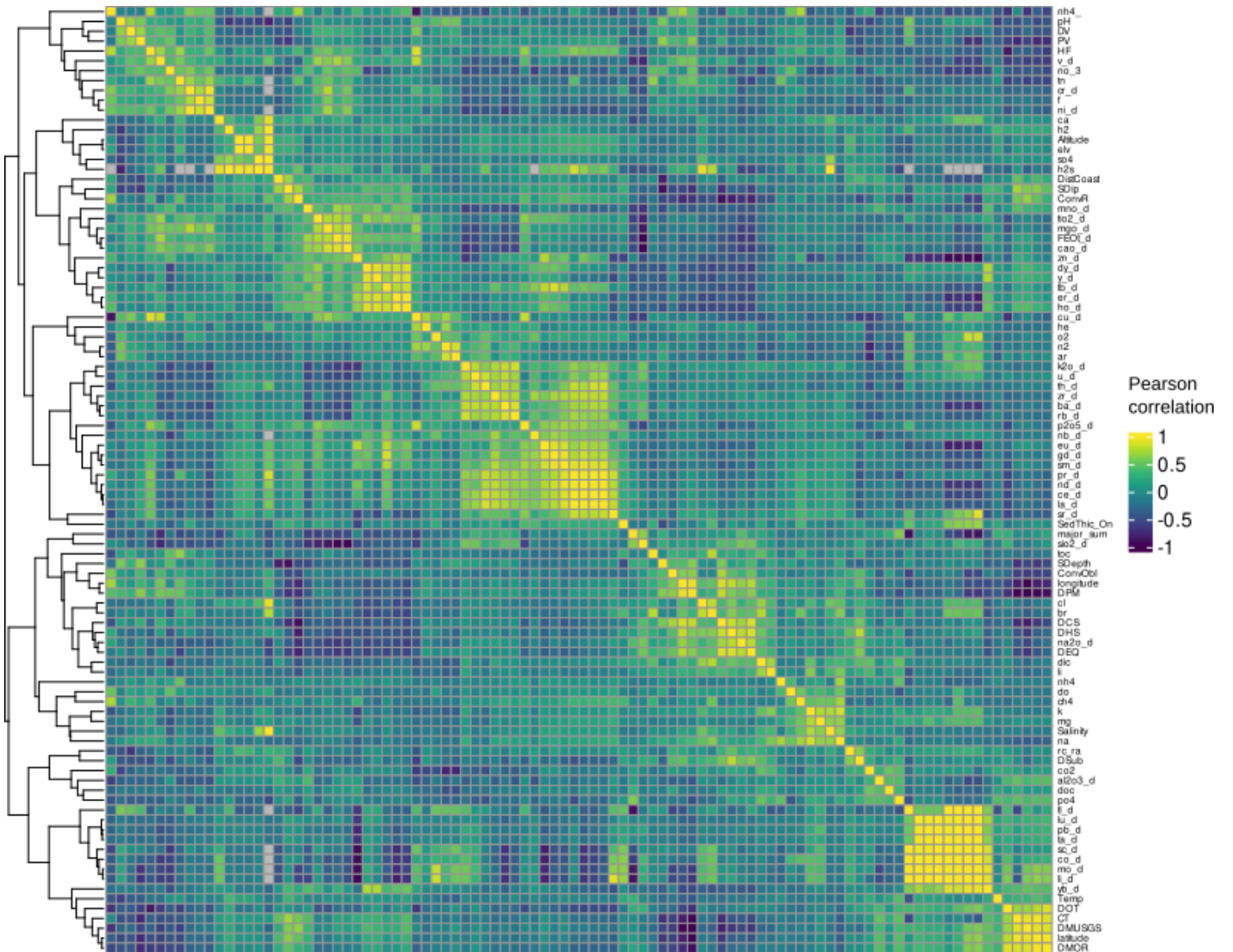
Supplementary Fig. S2. Changes in Temperature (A), pH (B) and $^3\text{He}/^4\text{He}$ (C) among the different sampled regions. One star (*); p-value less than 0.05, two stars (**) p-value is less than 0.01 and if p-value is less than 0.001, it is flagged with three stars (***)



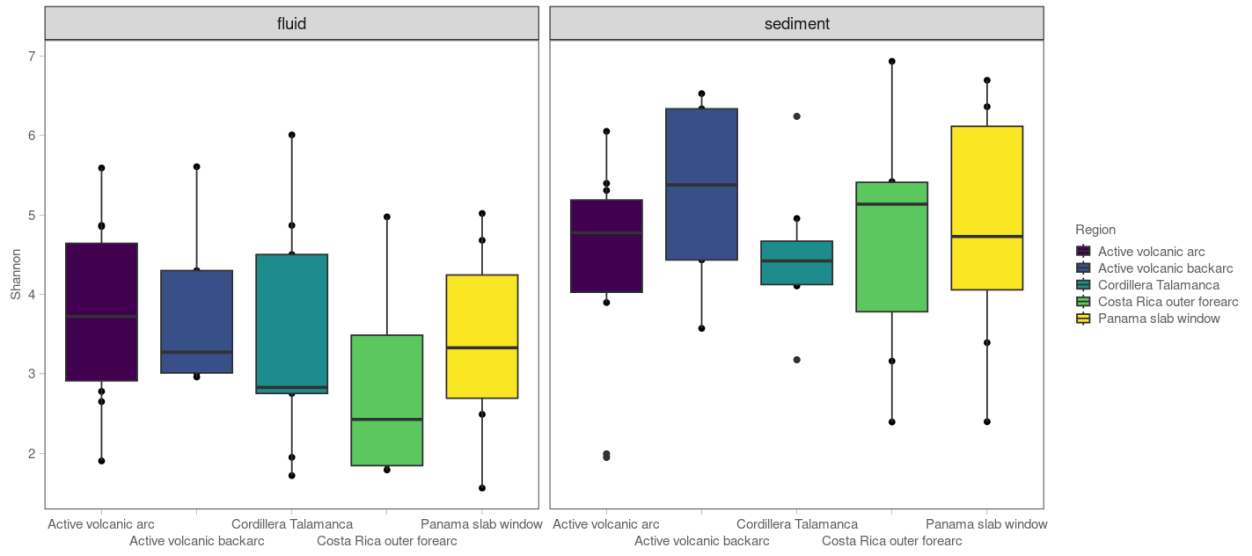
Supplementary Fig. S3. Ternary K-Na-Mg diagram after Giggenbach³ for evaluating the equilibrium temperature of representative fluid samples.



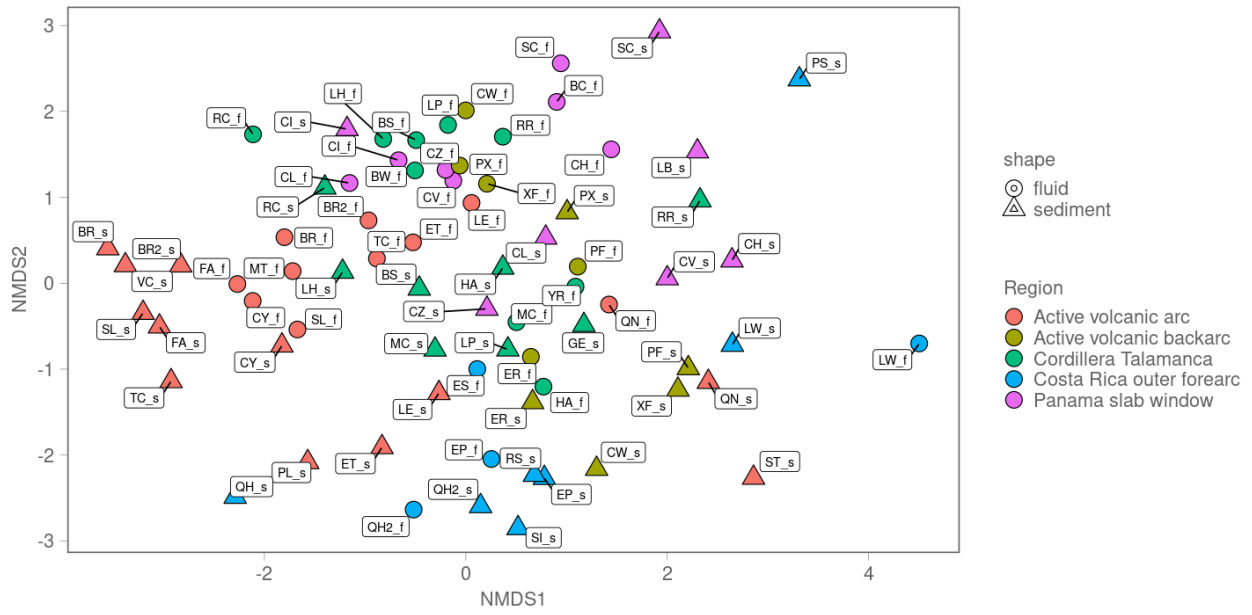
Supplementary Fig. S4. Matrix of correlation (Pearson correlation) among the environmental, geophysical, geochemical (major ions and trace element) variables showing collinearity among some of the investigated parameters.



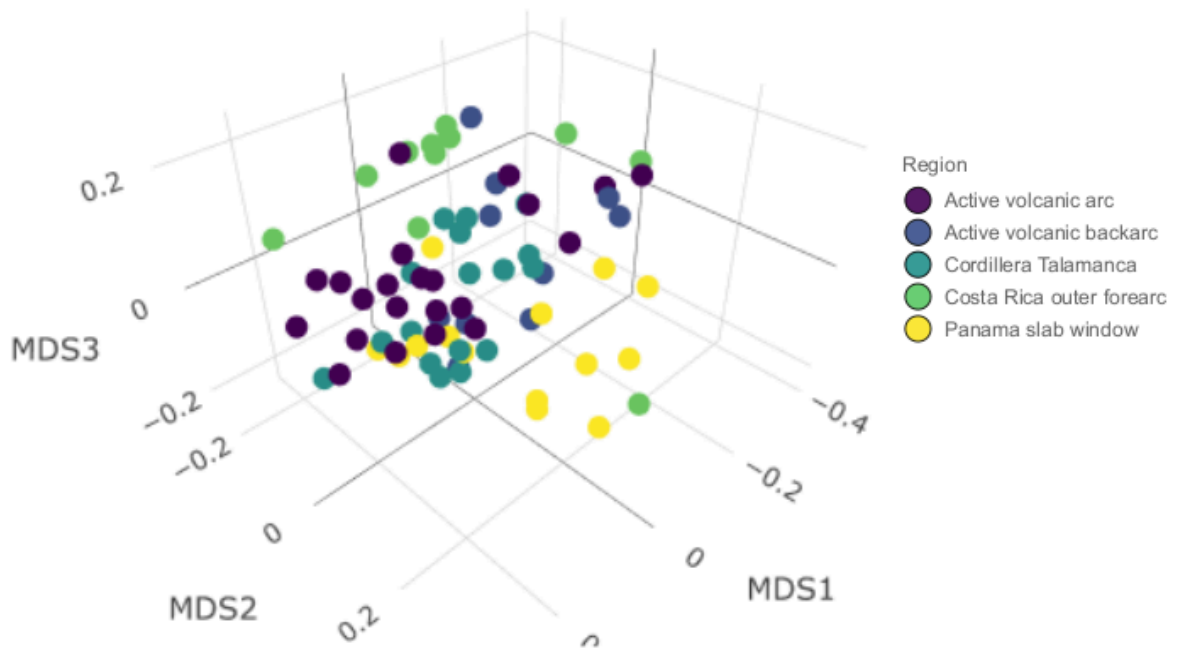
Supplementary Fig. S5. Shannon diversity metrics across geographical regions.



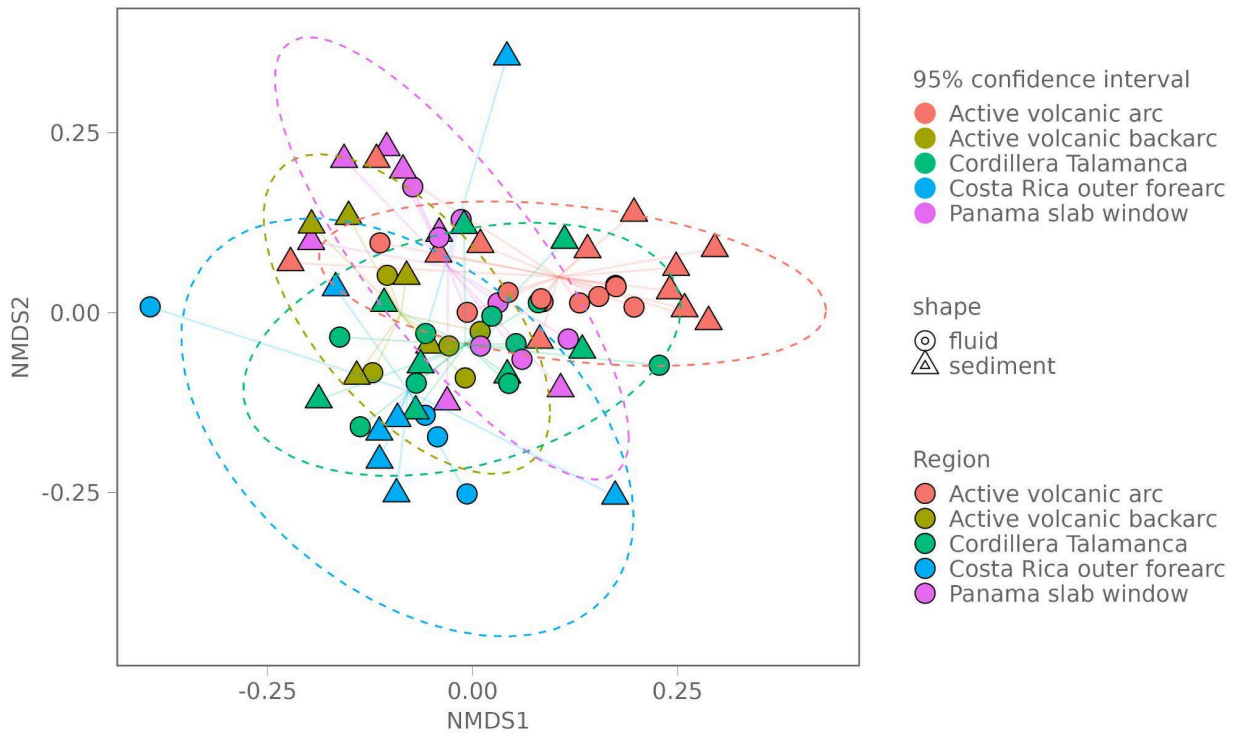
Supplementary Fig. S6. Non-metric multidimensional scaling (nMDS) plot based on the Jensen-Shannon Divergence colored by region with individual sites labeled.



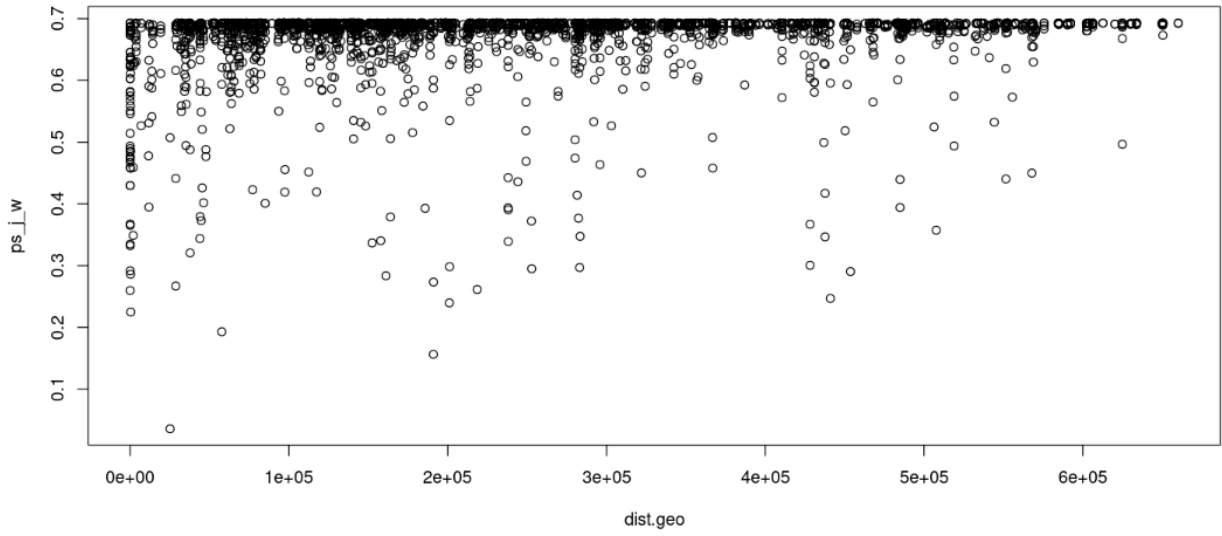
Supplementary Fig. S7. 3D view of the non-metric multidimensional scaling (nMDS) plot based on the Jensen-Shannon Divergence and colored by region.



Supplementary Fig. S8. Non-metric multidimensional scaling (nMDS) plot based on the weighted Jensen-Shannon Divergence coloured according to region (ellipses represent the 95% confidence interval of the group scoring).



Supplementary Fig. S9. Correlation between the Jensen-Shannon Divergence matrix and the pairwise geographical distance matrix to test for spatial autocorrelation.



Supplementary Fig. S10. Non-metric multidimensional scaling (nMDS) plot on the Jensen-Shannon Divergence distance between samples (stress = 0.17). Arrows show significant ($p < 0.05$) envfit results grouped by type of variables.

